

Relaxation Maps in Magnetic Resonance Imaging of Mouse Brain

A Thesis

submitted to

Indian Institute of Science Education and Research Pune in partial fulfilment of
the requirements for the BS-MS Dual Degree Programme

by

Ashrith Jacob



Indian Institute of Science Education and Research Pune
Dr. Homi Bhabha Road,
Pashan, Pune 411008, INDIA.

April, 2020

Supervisor: Prof. Dr. Dieter Suter

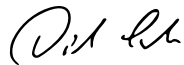
Ashrith Jacob

All rights reserved

Certificate

This is to certify that this dissertation entitled "Relaxation Maps in Magnetic Resonance Imaging of Mouse Brain" toward the partial fulfilment of the BS-MS dual degree programme at the Indian Institute of Science Education and Research, Pune represents study/work carried out by Ashrith Jacob at Technische Universität, Dortmund under the supervision of Prof. Dr. Dieter Suter, Professor at the department of Experimental Physics, TU Dortmund during the academic year 2019-2020.

Signature of Supervisor:



Signature of Student:



Declaration

I hereby declare that the matter embodied in the report entitled "Relaxation Maps in Magnetic Resonance Imaging of Mouse Brain" are the results of the work carried out by me at the Department of Experimental Physics, Technische Universität, Dortmund, under the supervision of Prof. Dr. Dieter Suter and the same has not been submitted elsewhere for any other degree.

Signature of Supervisor:

Dieter Suter

Signature of Student:

Alith

Acknowledgement

I would like to thank Prof. Dr. Dieter Suter for allowing me the great opportunity to explore a completely new field in Magnetic Resonance Imaging and his constant guidance and help throughout the thesis. I have learnt many invaluable traits regarding discipline and work ethic, through him. I would also like to thank Mrs. Sarah Belletz for helping me negotiate a complicated visa process for my arrival in Germany. My heartfelt gratitude to the other members of the laboratory, namely Fabian Kesselmann, Anna Dantas and Dr. Jingfu Zhang for their guidance and help, particularly with familiarising me with the experimental setup and for their help throughout the duration of the project. I also owe deep gratitude to my thesis committee member and project mentor over a number of semesters, Dr. TS Mahesh and Dr. Bijay Agarwalla. Their guidance over the previous two years has greatly enhanced my interest and helped me rediscover an interest in the physical sciences.

I thank my family for all their love and support without whom this journey would have been impossible. My eternal love to my friends for making this degree an adventure that I shall cherish for my lifetime. The boundaries of this thesis fall short to express my affection to my family and the IISER Pune community, but on closing note, 'For you a thousand times over'.

The financial support granted by TU Dortmund and through the KVPY scholarship is deeply appreciated.

Rather than love, than money, than fame, give me truth.

-Henry David Thoreau

CONTENTS

1 Abstract	11
2 Introduction	12
3 Spin Relaxation	13
3.1 Classical Description	13
3.2 Semi-classical description	15
3.2.1 Relaxation in Homonuclear 2 spin systems:	19
4 Method	22
4.1 Software and Spectrometer	22
4.2 Pulse Sequences	22
4.2.1 Flash Imaging	23
4.2.2 FlashChem Imaging	24
4.2.3 Spinwarp Imaging	27
4.3 Cutmask	27
4.4 Fitting Process	29
4.5 Initial Conditions	29
4.6 Fit Quality	32
4.7 SINC Pulse calibration	32
5 Results	36
5.1 Parameter shorthand:	36
5.2 Image details:	36
5.3 T1 maps	37
5.3.1 T1 map at 400MHz Spectrometer	38
5.3.2 T1 map at 600MHz Spectrometer	40
5.4 T2 maps	46
5.5 $T2^*$ map	48
6 Discussion	51

6.1 Trends	51
6.2 Sources of Error	52
6.2.1 Rotation Error	53
7 Conclusion	55

LIST OF FIGURES

3.1 - BLUE : Precession about effective field - RED : Relaxation to-	
wards thermal equilibrium - DOTTED : Net Magnetisation. [14]	
.....	14
3.2 TOP : Two spins with dipolar coupling with isotropic tumbling=7.8ns,	
BOTTOM : Average over 300 such spins. [14]	16
3.3 T1 relaxation as measured by only auto relaxation(BLUE) and	
by the sum of auto and cross relaxation(RED)	20
4.1 Flash Imaging Pulse sequence [15]	23
4.2 FlashChem Imaging Pulse sequence. [15]	24
4.3 Comparison of a saturation curve fit to inversion recovery fit,	
highlighting how Inversion recovery better exploits subtle T1 dif-	
ferences better [15]	26
4.4 Spinwarp Pulse sequence [15]	27
4.5 A colour map of $ T1_{fminsearch} - T1_{fit} $ so as to compare the two	
fit functions in matlab. One notices almost no difference (within	
the sample), except at pixels around the boundaries of the brain,	
where the fit function is more accurate.	30
4.6 An example of free fitting parameters converging to a local min-	
ima and not the global minima of the least square fit in an in-	
version recovery fitting. SI is the Magnetic Signal and Twait is	
the evolution time for relaxation.	30
4.7 A more accurate fit for inversion recovery curve	31
4.8 High Resolution (512x512) Flash image, TE(echotime)=20ms ..	33
4.9 Low Resolution (32x32) Flash image, TE(echo time)=20ms. Four	
points chosen from the blue(Brain) and four from the yellow(formalin). 33	
4.10 four pixels' Rabi Curve from region within the Brain	34
4.11 four pixels' Rabi Curve from region within the formalin	34
4.12 Average of the four pixels taken from within the region of the	
brain and formalin each. The sine Curve corresponding to the	
maximum value of the Rabi Curve. The more points are aver-	
aged, the better the curve fits the data points. One also observes	
a larger signal from the formalin as compared to the brain[see	
discussion].	35

5.1 T1 map (in seconds) using Flash at 400MHz, with detailed contrast	38
5.2 T1 map(in seconds) using Flash at 400MHz, with lower contrast. SITk=0.4mm	38
5.3 Signal Image for Twait of 20ms ,(Flashchem) at 600MHz. SITk=0.5mm, FrSl=0.0Hz	40
5.4 T1 map(in seconds) of the above slice using Inversion Recovery (Flashchem) at 600MHz	40
5.5 Histogram of the above T1 map. We notice two large bins:0.70-0.75s and 2.45-2.5s	41
5.6 T1 Fit of the two primary regions(Brain and Formalin) that we observe. Average RMSE=0.11	41
5.7 Signal Image for Twait of 400ms ,(Flashchem) at 600MHz. SITk=1.0mm, FrSl=-4000.0Hz	42
5.8 T1 map(in seconds) using Inversion Recovery (Flashchem) at 600MHz	42
5.9 Histogram of the above T1 map. We notice roughly four large bins:0.45-0.5s (white matter) and 0.7-0.8s(grey matter) , 1.6s and a peak beyond 2s(formalin).	43
5.10 T1 Fit of the two primary regions that we observe. Average RMSE=2.83	43
5.11 Signal Image for Twait of 20ms ,(Flashchem) at 600MHz. SITk=0.5mm, FrSl=0.0Hz	44
5.12 T1 map(in seconds) using Saturation Recovery (Flashchem) at 600MHz	44
5.13 Histogram of the above T1 map. We notice roughly two large bins:0.9-0.95s (Brain) and 1.3-1.35s. This could possibly correspond to the two middle peaks in figure 5.9. Since saturation recovery as previously mentioned, performs poorly in characterising different T1 values as compared to inversion recovery, we could expect this behavior(where certain peaks remain unresolved).	45
5.14 T1 Fit of the two primary regions that we observe. Average RMSE=1.27	45
5.15 Signal Image for TE of 12ms, (Spinwarp) at 600MHz. SITk=3.0mm, FrSl=-1500.0Hz	46
5.16 T2 map(in seconds) using Spinwarp at 600MHz	46

5.17 Histogram of the above T2 map. We notice two prominent bins: one at 15-17ms from the region in the Brain and another 30- 35ms from the region of the formalin.	47
5.18 T2 Fit of the two primary regions that we observe. RMSE=0.12	47
5.19 Signal Image for TE=20ms , Flash at 600MHz. SITk=1.0mm, FrSl=- 4000.0Hz	48
5.20 T2* map(in seconds) using Flash at 600MHz	48
5.21 Histogram of the above T2* map. We notice just a single peak at 20-25ms.	49
5.22 T2* Fit of the central region that we observe. RMSE=1.19	49
5.23 Plot fit 2	50
5.24 Plot fit 3	50
6.1 Markers used to track rotations	53
6.2 X pixel changes over different acquisitions (twait values).	54
6.3 Y pixel changes over different acquisitions (twait values). At larger twait times, the pixel moves almost a millimeter in dis- tance (sixteen pixels). This problem was eventually resolved by securing the tube in place within the probe head.	54

1 ABSTRACT

Magnetic Resonance Imaging relies on the nuclear spins of atoms within the tissue to produce an image of the tissue, under study. For imaging purposes, the Hydrogen atom nuclear spin is used because of its abundance in water and lipids which comprises a major part of tissues. In order to image tissues, certain gradient echo sequences, (such as Fast Low Angle Shot (FLASH)) and spin echo sequence (Spinwarp) are used to excite the spins within the tissue and develop an image, based on only magnetic signal from each individual voxel. This, however; is only the most basic, in a myriad possible methods, to image a tissue and distinguish it's various facets for medical diagnostics.

Each sequence type used in imaging, seeks to resolve the tissue imaging and bring about a contrast through a particular relaxation parameter such as T_1 , T_2 or T_2^* (longitudinal, transverse and apparent transverse spin relaxation times, respectively). On the other hand, diffusion of water and blood within the tissue structure can often lead to artefacts while imaging. This diffusive nature however is exploited in Diffusion Tensor Imaging(DTI) [1] and Diffusion Weighted Imaging (DWI) [2], where the regions are mapped through the diffusion coefficient of water, within the sample.

In this thesis we cover only relaxation maps (T_1 , T_2 , T_2^* maps). We explore the methodology of such measurements, the software and algorithms implemented and the contrast that such T maps can provide us with, in brain imaging. We hope to make observations and connect them to literature that could be the most possible explanation for the image contrasts observed.

Through this thesis we would like to consider the effectiveness of such T maps in distinguishing between tissues and hence have considered a suitable sample:the mouse brain. The brain of a mouse, having great similarity to those of humans, are also comprised of two primary tissues: Grey and White matter. This, thus forms a perfect sample to test the contrast mechanisms of such T maps.

2 INTRODUCTION

Magnetic Resonance Imaging is a technique by which images of tissues are constructed by means of magnetic signals from nuclear spins of atoms, constituting the tissues. In clinical and research MRI, hydrogen atoms are most widely used. This is due to an abundance of hydrogen atoms in water and lipids that constitute a majority of tissue structures.

MRI scans incorporate strong magnetic fields, magnetic gradients and radio frequency pulses to manipulate nuclear spins. This magnetic signal (from the nuclear spin ensemble) is further developed into the final MRI image, through different 'weightings'.

Images from MRI scans are weighted to encapsulate greater information regarding the tissue as well as form a method to develop contrasts between different tissues.

There are a number of different maps used in this thesis, they include:

- T1 maps
- T2 maps
- $T2^*$ maps

3 SPIN RELAXATION

An all encompassing literature guide for spin-lattice relaxation can be found here [8]. I will highlight a few facets of this below.

3.1 CLASSICAL DESCRIPTION

This classical description of spin relaxation through the Bloch Equations [3]:

$$\frac{d\mathbf{M}}{dt} = -\gamma\mathbf{B} \times \mathbf{M} - \mathbf{R}[\mathbf{M}(\mathbf{t}) - \mathbf{M}_{eq}] \quad (3.1)$$

Where, \mathbf{B} is the applied external magnetic field and \mathbf{M} is the magnetisation vector. There are two time dependant factors:

- Precession about effective field.
- Relaxation towards Equilibrium.

The solution for initial conditions, $\mathbf{M}(\mathbf{0})=(0, 0, M_o)$; $\mathbf{B}(\mathbf{0})=(0, 0, B_o)$ for [3.1], where (x, y, z) are the standard cartesian coordinate system notation to represent the X, Y and Z coordinates respectively.

$$\mathbf{M}(\mathbf{t}) = \mathbf{R}_z(-\gamma B_o t) e^{-\mathbf{R}t} [\mathbf{M}(\mathbf{0}) - \mathbf{M}_{eq}] + \mathbf{M}_{eq} \quad (3.2)$$

Where the relaxation matrix,

$$\mathbf{R} = \begin{bmatrix} 1/T2 & 0 & 0 \\ 0 & 1/T2 & 0 \\ 0 & 0 & 1/T1 \end{bmatrix}$$

T1 is the longitudinal spin relaxation time constant, as the longitudinal spin magnetisation approaches its equilibrium value and T2 is the axial spin relaxation time constant as the axial spin magnetisation approach zero. It is important to note that between the two relaxation rates, T1 (longitudinal spin relaxation rate) and T2 (the axial spin relaxation rate) differ in the fact that T1 changes the energy of the system, while T2 does not. There is also a constraint on the ratio of T1:T2, where $T1 \geq T2/2$ [4].

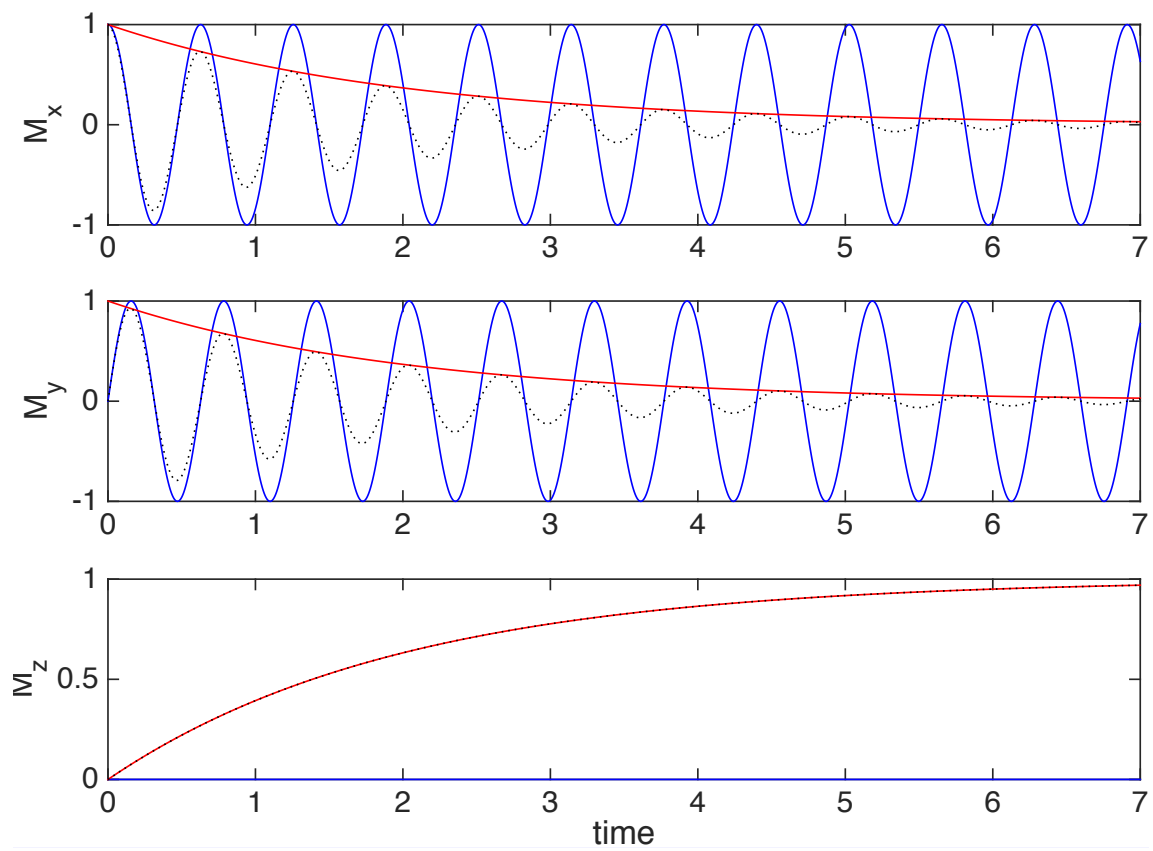


Figure 3.1: -**BLUE**: Precession about effective field -**RED** : Relaxation towards thermal equilibrium -**DOTTED** : Net Magnetisation. [14]

3.2 SEMI-CLASSICAL DESCRIPTION

The semi classical description is given by the Redfield relaxation theory, also known as the WBR (Wangsness, Bloch, Redfield) theory. This theory is based on the stochastic motion of molecules due to rotational tumbling and other processes in liquid and solids [5] [6] [7].

We begin by considering the laboratory framed Hamiltonian:

$$\mathbf{H}(t) = \mathbf{H}_0 + \mathbf{H}_1(t) \quad (3.3)$$

Where: We have the static, deterministic part that contains the Zeeman term (Z), isotropic chemical shifts (CS) and J couplings (J) represented respectively in [3.4]

$$H_o = H_Z + H_{CS} + H_J \quad (3.4)$$

The stochastic part includes second-ranked terms like the dipole coupling (D), the quadrupolar coupling (Q) and the chemical shift anisotropy (CSA).

$$H_1(t) = H_D(t) + H_{CSA}(t) + H_Q(t) \quad (3.5)$$

The Liouville-von Neumann equation gives the time evolution of the spin density function, $\sigma(\vec{t})$:

$$\frac{d}{dt}\sigma(\vec{t}) = -i[H(t), \sigma(\vec{t})] = -i[H_o + H_1(t), \sigma(\vec{t})] \quad (3.6)$$

The stochastic, time-dependent part of the Hamiltonian results in a different time evolution of each spin, but averaged over an ensemble shows a fairly accurate monoexponential behaviour with the expected time constant (see [3.2]).

In order to solve equation [3.6] (with the the stochastic time-dependent operator), we can, through second order perturbation theory, arrive at:

$$\frac{d}{dt}\sigma(\vec{t}) = -i[H_o(t), \sigma(\vec{t})] - \hat{\Gamma}\{\vec{\sigma}(t) - \vec{\sigma}_{eq}\} \quad (3.7)$$

Where, $\hat{\Gamma}$ is the relaxation super operator. In the derivation of the *master equation* [3.7], the assumptions made are as follows:

- The Stochastic Hamiltonian is a bias free perturbation
- The ad hoc introduction of relaxation towards a finite thermal equilibrium ensures that the relaxation super operator is symmetric.

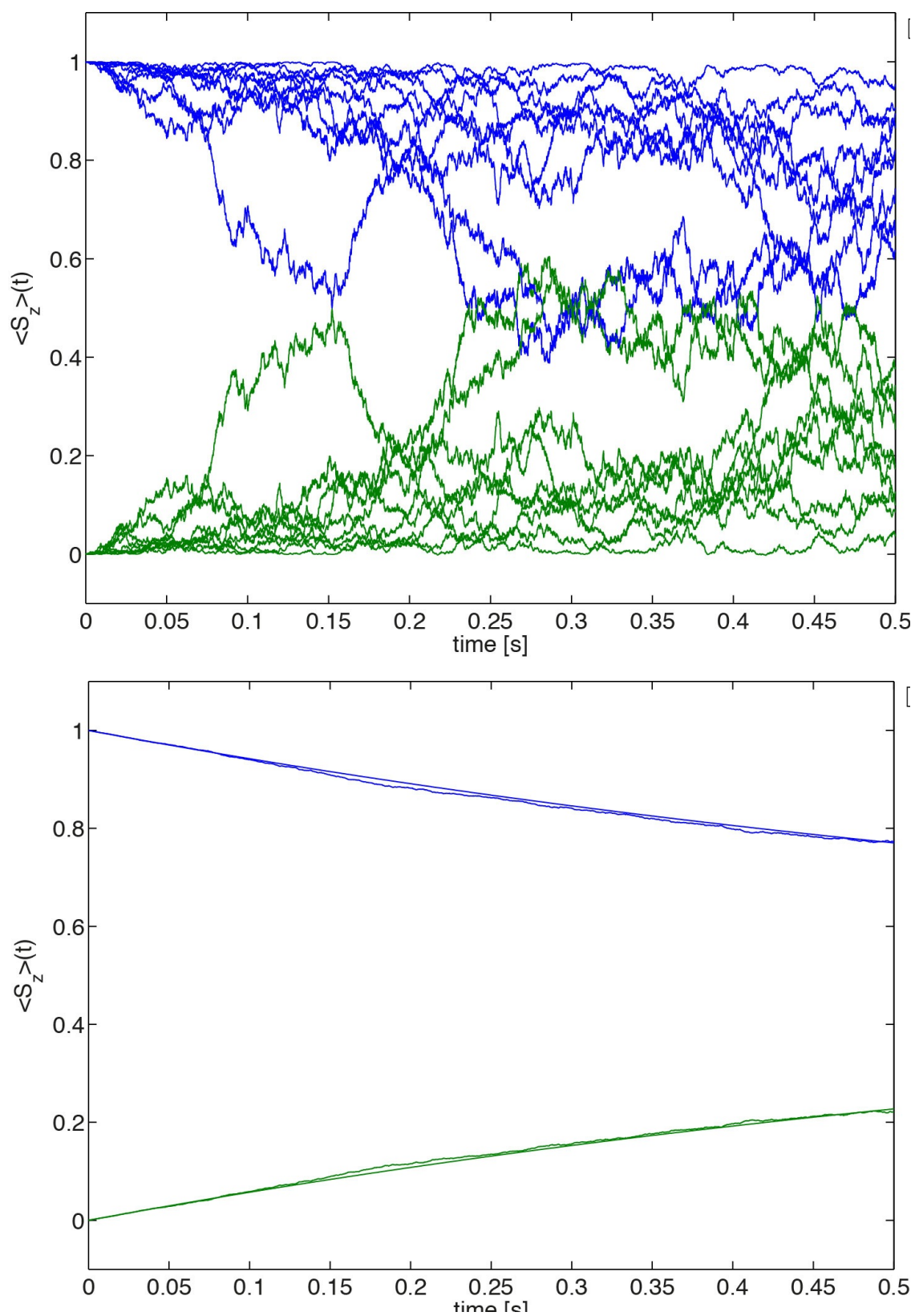


Figure 3.2: **TOP:** Two spins with dipolar coupling with isotropic tumbling=7.8ns, **BOTTOM:** Average over 300 such spins. [14]

- The random fluctuations is much shorter, in scale than changes in the density operator (Redfield limit).

Converting [3.6](#) into the interaction-frame [\(3.8\)](#), we eliminate the deterministic part and are left with the purely stochastic element of the Hamiltonian that is responsible for time evolving the density operator.

$$\frac{d}{dt}\hat{\sigma}(t) = -i[\hat{H}_1(t), \hat{\sigma}(t)] \quad (3.8)$$

Where, $\hat{H}_1(t) = e^{+iH_0t} H_1 e^{-iH_0t}$ and $\hat{\sigma}(t) = e^{+iH_0t} \sigma(t) e^{-iH_0t}$.

We solve the Liouville-von Neumann [\(3.8\)](#):

$$\frac{d}{dt}\hat{\sigma}(t) = i[\hat{\sigma}(0), \hat{H}_1(t)] - \int_0^t [\hat{H}_1(t), [\hat{H}_1(t^1), \hat{\sigma}(t^1)]] dt^1 \quad (3.9)$$

Where the solution:

$$\hat{\sigma}(t) = \hat{\sigma}(0) - i \int_0^t [\hat{H}_1(t^1), \hat{\sigma}(t^1)] dt^1 \quad (3.10)$$

was plugged back into the differential equation [\(3.8\)](#) to produce the second order differential equation. On replacing $t^1 = t - \tau$, to adjust integration boundaries, we get:

$$\frac{d}{dt}\hat{\sigma}(t) = i[\hat{\sigma}(0), \hat{H}_1(t)] - \int_0^t [\hat{H}_1(t), [\hat{H}_1(t - \tau), \hat{\sigma}(t - \tau)]] d\tau \quad (3.11)$$

On taking the ensemble average of equation [\(3.10\)](#), we get $\langle [\hat{\sigma}(0), \hat{H}_1(t)] \rangle = 0$ (assuming that the stochastic process is unbiased). This leads to the simplified form of Liouville-von Neumann [\(3.8\)](#):

$$\frac{d}{dt} \langle \hat{\sigma}(t) \rangle = - \int_0^t \langle [\hat{H}_1(t), [\hat{H}_1(t - \tau), \hat{\sigma}(t - \tau)]] \rangle d\tau \quad (3.12)$$

The next step is to introduce thermal equilibrium conditions, which at it's present form is $\langle \sigma_{eq} = 0 \rangle$, assuming at it's present form an equilibrium condition of $T = \infty$. Adding this adhoc equilibrium condition corrects that the super operator is symmetric which assumes infinite temperature. Therefore we arrive at an inhomogenous equation:

$$\frac{d}{dt} \langle \hat{\sigma}(t) \rangle = - \int_0^t \langle [\hat{H}_1(t), [\hat{H}_1(t - \tau), \hat{\sigma}(t - \tau) - \sigma_{eq}]] \rangle d\tau \quad (3.13)$$

Now, we note that the LHS and RHS of [3.13](#) is at different times and if τ is much smaller than the time scale over which the density matrix varies, then

we can replace $t - \tau$ by t . This is commonly referred to as the Redfield limit or weak collision limit, which hold true and valid in NMR systems. We then have:

$$\frac{d}{dt} \langle \hat{\sigma}(t) \rangle = - \int_0^t \langle [\hat{H}_1(t), [\hat{H}_1(t), \hat{\sigma}(t) - \sigma_{eq}]] \rangle d\tau \quad (3.14)$$

which leads us back to [3.7](#), where $\hat{\Gamma}$ is the relaxation super operator, where the operator is defined as:

$$\hat{\Gamma}\{Q\} = \int_0^t \langle [\hat{H}_1(t), [\hat{H}_1(t - \tau), Q]] \rangle d\tau \quad (3.15)$$

We now proceed to write the Hamiltonians in spherical tensor terms.

$$H = \sum_{\mu, l, m} (-1)^m A_{l, -m}^\mu \hat{T}_{l, m}^\mu \quad (3.16)$$

We then by algebraic manipulations and certain assumptions [9](#) [10](#) arrive at:

$$\Gamma\{\hat{Q}\} = \frac{1}{2} \sum_{\mu, \mu^1, l, m, p^1} [\hat{\mathbf{T}}_{l, m}^\mu, [(\hat{\mathbf{V}}_{p^1}^{\mu^1})^\dagger, \hat{Q}] J_{l, l, -m, -m}^{\mu, \mu^1}(\omega_{p^1}) \quad (3.17)$$

Here there are primarily two terms of interest:

- Double commutator term: in **boldfont**- specifies the relaxation pathway.
- spectral density term (J)- specifies the strength of such a pathway.

$$\text{Where: } C_{l, l^1, -m, -m^1}^{\mu, \mu^1}(\tau) = A_{l, -m}^\mu(t) (A_{l^1, -m^1}^{\mu^1})^*(t - \tau)$$

$$\text{and replacing } e^{-iH_0\tau} (\hat{\mathbf{T}}_{l^1, m^1}^{\mu^1})^\dagger e^{+iH_0\tau} = \sum_p (\hat{\mathbf{V}}_p^\mu)^\dagger e^{i\omega_p\tau}$$

by taking time t to ∞ and by replacing:

$$J_{l, l, -m, -m}^{\mu, \mu^1}(\omega_{p^1}) = 2 \int_0^\infty C_{l, l^1, -m, -m^1}^{\mu, \mu^1}(\tau) e^{i\omega_{p^1}\tau} d\tau$$

The **boldfont** term in [3.17](#), as mentioned above specifies the relaxation pathway, more specifically which relaxation pathways are allowed. Different spherical-tensor operators, involved in the double commutator allows for different relaxation pathways. If $\mu = \mu^1$, it's called auto-correlation relaxation or else if $\mu \neq \mu^1$, it's called cross-correlation relaxation. The auto correlation term, is the diagonal term in the relaxation superoperator and relates to a loss of coherence/polarisation. Likewise, the cross-correlation term (off diagonal terms of the superoperator), is the transference of one coherence to another.

The spectral-density function depends on the model of motion that generates the stochastic modulation of the Hamiltonian. These are the Fourier Transforms of the correlation function of the spatial tensor components. Since the simplest stochastic processes are described by an exponential decay correlation, the simplest model is isotropic rotational tumbling is a Lorentzian:

$$J(\omega) = \frac{2}{5} \frac{\tau}{1 + (\omega\tau)^2} \quad (3.18)$$

This value of the spectral density function is dependent on both resonant frequency(ω) and correlation time(τ). If $(\omega\tau) \ll 1$ then we find $J(\omega) = J(0)$ and we consider this the extreme narrowing limit. This limit is approached at very low fields (therefore low frequency) and for small molecules(and hence lower τ).

Secular Approximation:

Key to the study of T1 and T2 relaxation, is the secular approximation, where we abstract the ideas of the above theory and make it more relevant to experimental observations in Magnetic Resonance Imaging. The Hamiltonian super operator has the Zeeman frequencies of the corresponding basis operators on the diagonal. If the difference in Zeeman frequency of the two basis operators is much larger than the off diagonal element, the cross relaxation is eliminated. Additionally, for a number of relaxation mechanisms such as dipolar,quadrupole, CSA the commutators also do not allow cross relaxation between different coherence orders.

3.2.1 RELAXATION IN HOMONUCLEAR 2 SPIN SYSTEMS:

Since most MRI experiments, as well as all carried out by myself in the thesis relies on nuclear spins of hydrogen nuclei, alone, we consider the monoatomic case, which is the less general case, but applicable to this thesis. We consider only the auto-correlated CSA and dipolar relaxation and at cross-correlated dipolar/CSA relaxation. We, additionally ignore quadrupolar relaxation. Now, calculating the superoperator, $\hat{\Gamma}\{Q\}$ from [3.17](#) where $Q = S_Z$, we get:

$$\hat{\Gamma}_{I_Z I_Z} = \left(\frac{\delta}{4}\right)^2 [J(0) + 3J(\omega) + 6J(2\omega)] \quad (3.19)$$

Where the dipolar coupling for a hydrogen molecule: $\delta = -2 \frac{\mu}{4\pi} \frac{\gamma_H^2 \hbar}{r_{HH}}$.

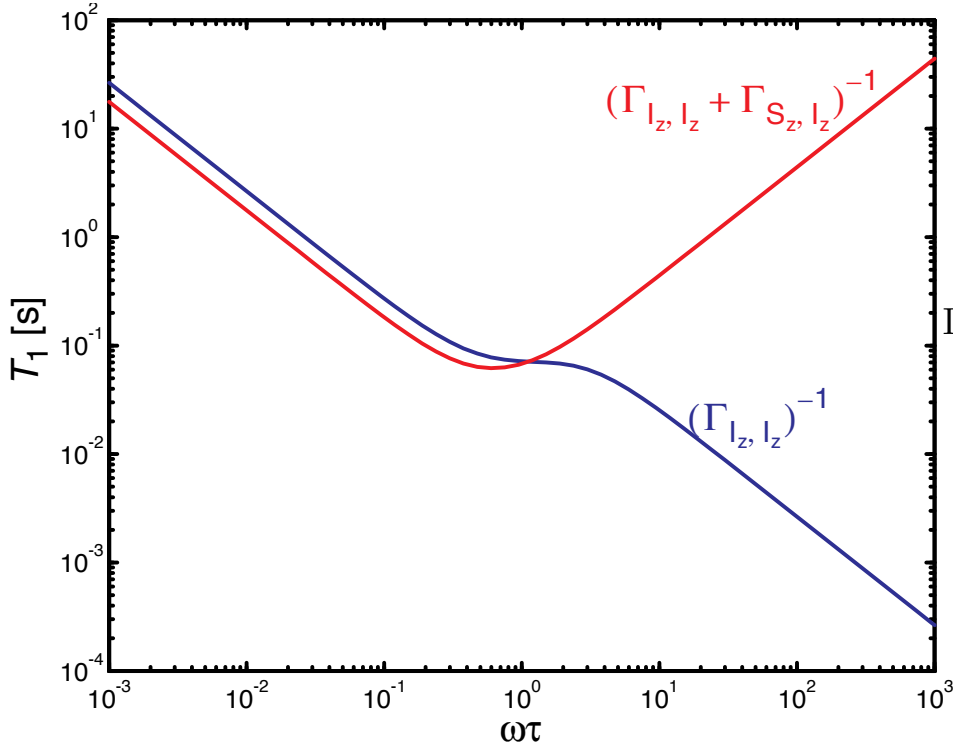


Figure 3.3: T1 relaxation as measured by only auto relaxation(BLUE) and by the sum of auto and cross relaxation(RED)

The longitudinal relaxation time, T1 relates to this superoperator as it's inverse, therefore we have:

$$\frac{1}{T1} = \left(\frac{\delta}{4}\right)^2 [J(0) + 3J(\omega) + 6J(2\omega)] \quad (3.20)$$

Where $J(\omega)$ is given by equation [3.18](#).

It is experimentally really difficult to measure the T1 of a single homonuclear spin. It is usually easier to measure the relaxation property (in this case of T1) of the ensemble net magnetisation, which is the total proton magnetisation. This is the sum of both auto as well as cross relaxation models. Thus the actual measured T1 is the sum of both these terms:

$$\frac{1}{T1_{measured}} = \hat{\Gamma}_{I_z I_z} + \hat{\Gamma}_{S_z I_z} = \left(\frac{\delta}{4}\right)^2 [J(0) + 3J(\omega) + 6J(2\omega)] + \left(\frac{\delta}{4}\right)^2 [-J(0) + 6J(2\omega)] \quad (3.21)$$

The trends in T1 vs $\omega\tau$ are represented in figure [3.3](#)
Similar analysis for T2 relaxation gives us:

$$\frac{1}{T2} = \Gamma_{S^+, S^+} = \left(\frac{\delta}{4\sqrt{2}}\right)^2 (5J(0) + 9J(\omega) + 6J(2\omega)) + \frac{(\delta_S)^2}{2} (J(0) + \frac{3}{4}J(\omega_S)) \quad (3.22)$$

The second term is due to Chemical shift anisotropy and δ_S the associated constant. On comparing the T1 and T2 plots it is observed that T1 decreases

as a function of the tumbling rate ($\omega\tau$), but then increases beyond a threshold value, which is generally near Larmor frequency (order of magnitude). T_2 however continuously decreases with increased tumbling rate. [3.3](#) and demonstrates graphically these trends.

4 METHOD

4.1 SOFTWARE AND SPECTROMETER

The experiments were conducted at the 600MHz spectrometer at the experimental physics department at TU, Dortmund. A couple of experiments were also performed at the 400MHz.

The software at the 600MHz is Spinsight, which was released by Varian, while the software used at the 400MHz is a preclinical software known as Paravision, produced by Bruker.

4.2 PULSE SEQUENCES

There are primarily three pulse sequences that were used in this thesis to produce the maps. They include:

- Flash Imaging
- FlashChem Imaging
- Spinwarp Imaging

These pulse sequences were part of the software Spinsight at the 600MHz spectrometer.

4.2.1 FLASH IMAGING

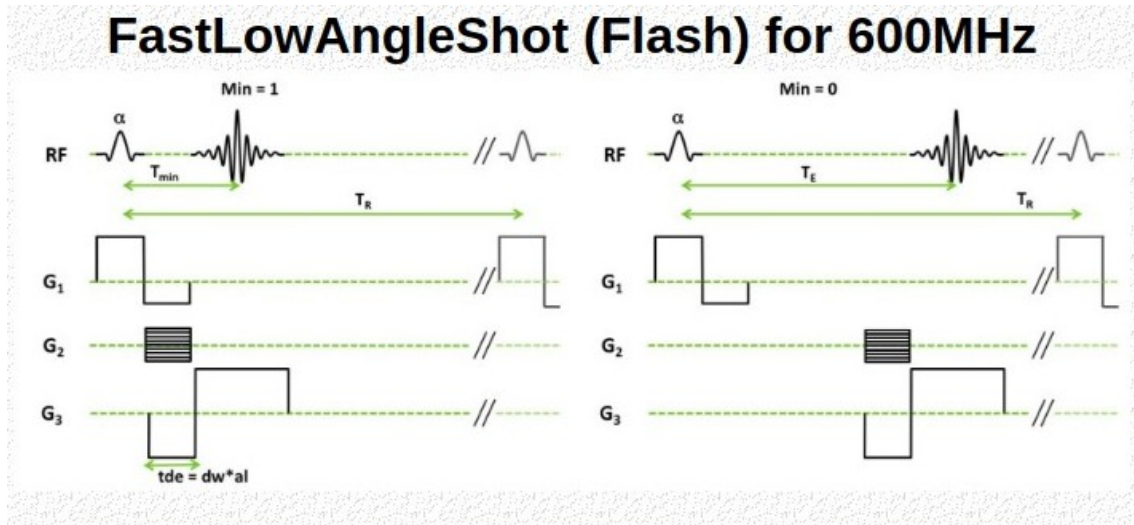


Figure 4.1: Flash Imaging Pulse sequence [15]

This Pulse sequence relies on gradient echo pulse sequence. The numbers(1,2,3) correspond to planes(x,y,z) respectively, along which the gradients are applied.

The important difference between conventional imaging techniques and this rapid sequence is the use of radio frequency pulses with low flip angles. It is based on the acquisition of the free induction decay in the form of a gradient echo generated by reversal of the read gradient. The entire imaging time is only given by the number of projections desired, times the duration of slice selection and data acquisition. Since the FTD requires only a single excitation pulse(with a flip angle of α), this type of signal turns out to be best-suited for rapid NMR imaging. Frequency and phase readout help form a k space data set, which is a result of repeating the sequence, for different spatial encodings. This k space data is then processed by means of a custom made matlab script to give magnetic signal maps. Here, a number of factors determine the magnetic signal of the image and is described by:

$$S = K[H] \frac{\sin(\alpha)(1 - e^{-\frac{TR}{T_1}})}{(1 - \cos(\alpha)e^{-\frac{TR}{T_1}})} e^{-\frac{TE}{T_2^*}} \quad (4.1)$$

K[H]: proportionality constant based on Hydrogen atom concentration in sample slice.

α : Flip angle

The angle that maximises the signal is often chosen and is called the ernst angle.

$$\alpha_{ernst} = \cos^{-1}(e^{-\frac{TR}{T1}}) \quad (4.2)$$

The above relation can be easily derived by solving the first differential of S set to zero, in order to locate the maxima.

. The utility of Flash Imaging is varied with great utility to produce different maps:

- For $TR \gg T1$ and constant flip angle, α , we get a $T2^*$ map, by varying TE over a range of values and fitting an exponential curve.
- Similarly for $TE \ll T2^*$ and a flip angle of $\frac{\pi}{2}$, we could fit a saturation curve for a T1 map. Although this would simplify the fitting curve as per [4.1](#), the signal would be best at a flip angle corresponding to Ernst angle.

4.2.2 FLASHCHEM IMAGING

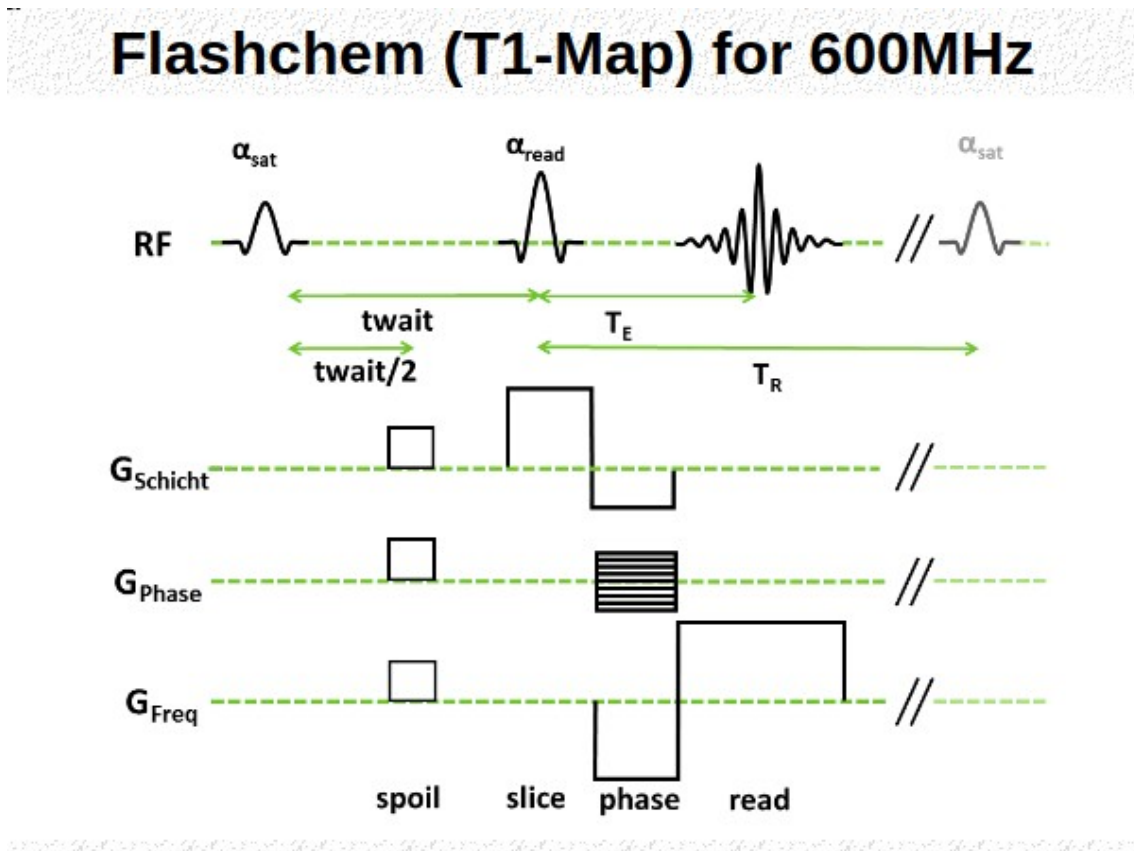


Figure 4.2: FlashChem Imaging Pulse sequence. [\[15\]](#)

This pulse sequence is similar to flash imaging with a saturation pulse (with flip angle, α_{sat}) prior to the flash imaging pulse (with flip angle, α_{read}).

Based on the values of the two flip angles, we could have different types of T1 maps:

- Saturation Recovery
- Inversion Recovery

Saturation Recovery

In this method $\alpha_{sat} = \frac{\pi}{2} = \alpha_{read}$. This leads to the net axial magnetisation increasing from 0 till it's maximum value (all magnetisation along the axial direction). The saturation recovery curve is of the form:

$$y = A(1 - e^{-\frac{t}{T1}}) \quad (4.3)$$

Inversion Recovery

In this method $\alpha_{sat} = \pi$ and $\alpha_{read} = \frac{\pi}{2}$. This leads to the magnitude of the axial magnetisation decreasing from its maximum value (when all the magnetisation is along the lower axial direction, due to the π pulse), till it's minimum value (zero) and a further increase to reach the equilibrium position with the net magnetisation along the upward axial direction. The inversion recovery curve fits a function of the general form:

$$y = |A - Be^{-\frac{t}{T1}}| \quad (4.4)$$

Inversion recovery is a more accurate fit to T1 relaxation maps as opposed to a saturation recovery fit.

The reason for these include:

- Selective tissue suppression: When the axial magnetisation is flipped to the negative z axis and returns to its original magnetisation, it passes through the zero magnetisation (along the axial Z direction). At this value of t_{wait} , that particular tissue produces no signal (is nulled). This value of $t_{wait} = T1 * \ln 2$
- Due to the time period of the evolution, one can exploit subtle differences in T1 values from an inversion recovery curve as it evolves over a larger range of magnetisation (see [4.3](#)).

Disadvantages of inversion recovery include:

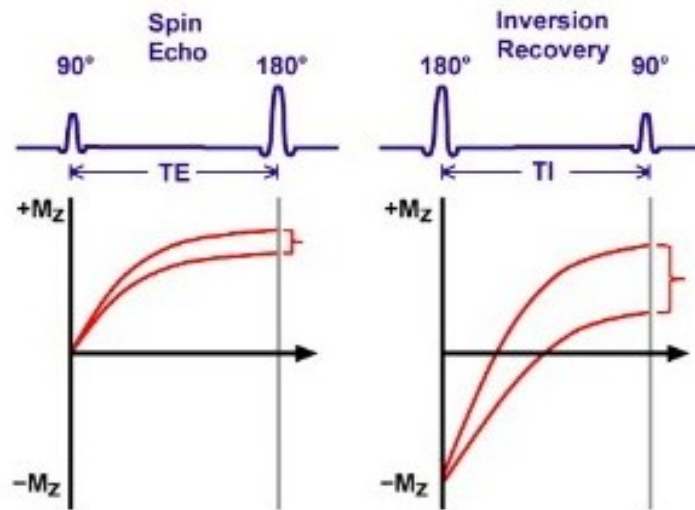


Figure 4.3: Comparison of a saturation curve fit to inversion recovery fit, highlighting how Inversion recovery better exploits subtle T1 differences better [15]

- Longer scan times.
- Larger SAR (specific absorption rate).

SAR represents the rate of absorption of the human body to energy when exposed to radio frequency pulse. In the context of MRI, we desire a lower level of SAR as this would be safer to implement in a clinical setup.

4.2.3 SPINWARP IMAGING

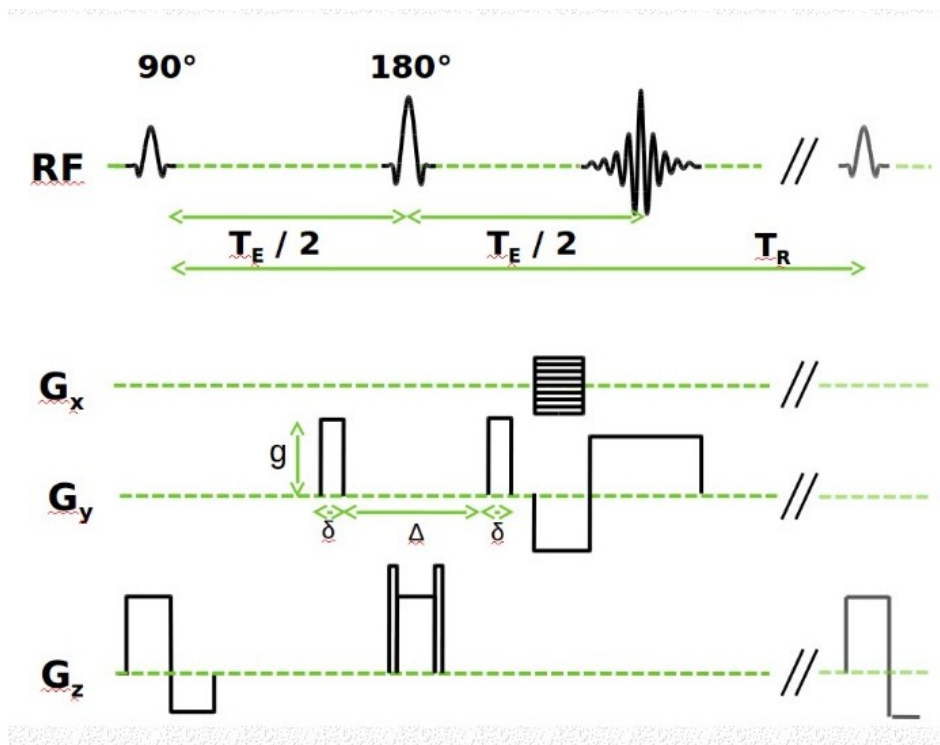


Figure 4.4: Spinwarp Pulse sequence [15]

This is a spin echo sequence rather than gradient echo. An excitation $\pi/2$ pulse is used to rotate the magnetization onto the longitudinal plane after which a π pulse is used to generate the spin echo.

This sequence is used to generate a T2 map, by increasing the echo time (TE). On doing so, a gradually weaker echo signal is generated. This drop in echo intensity follows an exponential curve, where:

$$M_{xy} = Ae^{-TE/T2} \quad (4.5)$$

M_{xy} , being the transverse magnetisation.

4.3 CUTMASK

All the images are processed through a number of matlab scripts that fulfil a certain task with respect to image processing.

A cutmask is a method to eliminate the noise in the T maps. This is done in two steps:

- Determine the noisy regions in the image (i.e where the SNR is low).

- Set these regions to NaN, where they do not interfere with the colour schemes of the final maps.

These functions are carried out by the method **cut2D.m** (creator: Fabian Kesselmann) located under the path:

StorageE3 \User \E3a \Research_Data_Management \Processing \Matlab.

This script sums up the magnetic signal from all images used in the map and based off a user defined cutoff value, sets the remaining points that are below the particular fraction of the maximum signal, to NaN. Thus the noisy surrounding outside the sample tube (that contains the brain sample), having the property of lower signal uniformly across all images are automatically eliminated through this algorithm.

4.4 FITTING PROCESS

Any T map is created by fitting each pixel in the image slice according to a particular relaxation curve. Thus, the higher the resolution, the more resolved the image is. For most images used in this thesis, we stick to a resolution of 256x256 pixels.

This pixel-wise fitting is done by acquiring a number of images(n) with different repetition/ echo / twait times(as the case might be) and fitting the corresponding curve to each pixel point from the magnetic signal acquired across all the 'n' images, we arrive at the fitting parameters corresponding to each pixel. One of the fitted parameters, being $T1, T2, T2^*$ allows us to assign this fitted parameter to each pixel and can be visualised via a colourmap.

To implement this pixel wise fitting, I had created a matlab method, **relaxation_fit_AJ.m** (creator:Ashrith Jacob) located under the path: **StorageE3\User\E3a\Research_Data_Management\Processing\Matlab**. This function lets the user input the type of fit required and it incorporates an inbuilt function, `fminsearch()` to optimise the free parameters of the fit. It's from these free parameters (namely $T1, T2$ and $T2^*$) that we are able to develop the corresponding maps.

There are a couple of inbuilt functions that can be utilised. Apart from **fminsearch()**, matlab provides a **fit()** function as well.

4.5 INITIAL CONDITIONS

The free parameters that are to be optimised pixel-wise tend to depend heavily on the starting parameters. We hope to optimise them to their global minima (where the root mean square error is lowest between the the fitted curve and data points). Arriving at this global minima is not guaranteed and the parameters could converge at a local minima instead.

This can be noticed particularly well in the case of an Inversion recovery curve. Due to a presence of a 'kink' (i.e not differentiable point), one can determine to an extend the accuracy of the fit by plotting the fitted curve for a pixel with its corresponding data points.

To overcome this problem in Inversion recovery, starting parameters are optimised. In inversion recovery, the fitted function follows the following equation:

$$SI = |A - Be^{-t/T1}| \quad (4.6)$$

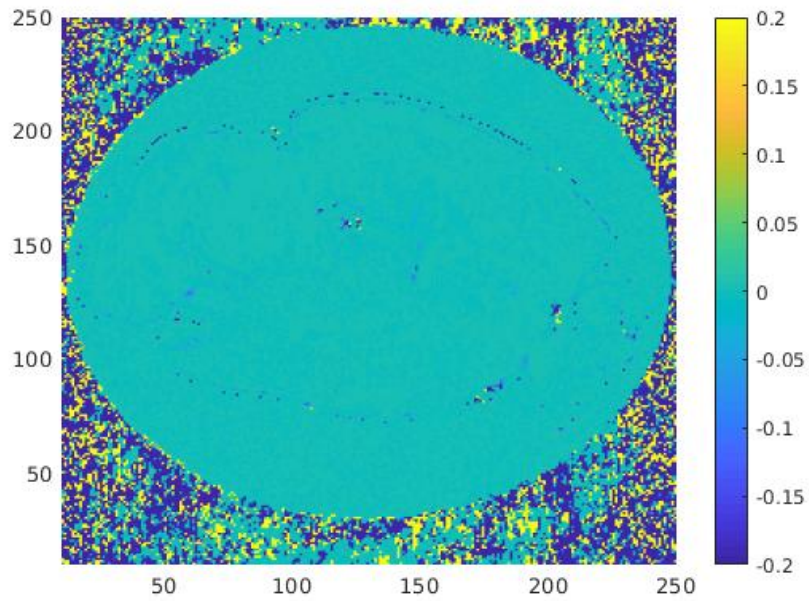


Figure 4.5: A colour map of $|T1_{fminsearch} - T1_{fit}|$ so as to compare the two fit functions in matlab. One notices almost no difference (within the sample), except at pixels around the boundaries of the brain, where the fit function is more accurate.

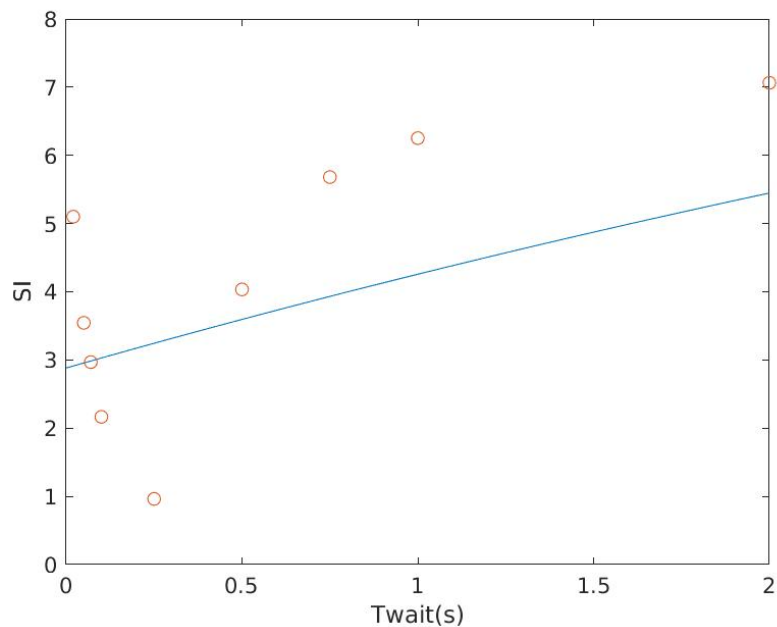


Figure 4.6: An example of free fitting parameters converging to a local minima and not the global minima of the least square fit in an inversion recovery fitting. SI is the Magnetic Signal and Twait is the evolution time for relaxation.

Where there exists three free parameters.

In order to optimise starting parameters, we choose values that would lie nearer to the predicted global minima. Since we know that at large times, the curve should approach the value of A , we can set A_{start} to the Signal corresponding to the largest evolution time. Similarly at evolution times closer to zero we expect signal to be $(B - A)$ and therefore set $B_{start} = A_{start} - (\text{signal at the shortest evolution time})$. This procedure is incorporated into `relaxation_fit_AJ.m`.

Although this seems like a reasonable solution to the decide the starting parameters, it remains to be verified if the values the fit converges to are really the global minimas. In order to verify this, we utilise an array of starting values and observe the final fitted values. By identifying the minimum least square value that was achieved and comparing it to the values that the previous method produced, we can confirm whether or not the free parameters actually converged to their global minima or not.

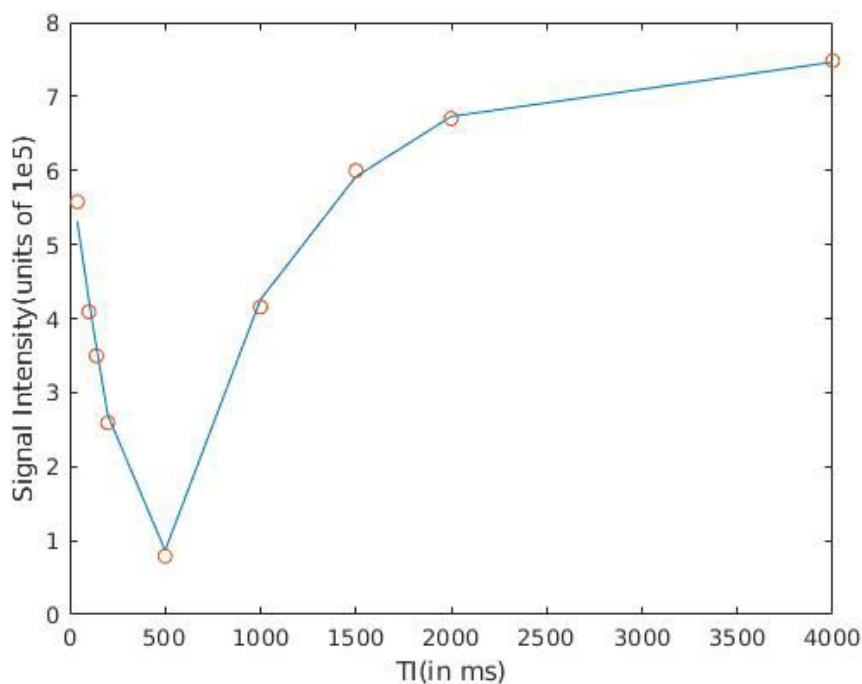


Figure 4.7: A more accurate fit for inversion recovery curve

The main script used to develop the histogram plots and call the aforementioned functions, is located at:

`\\StorageE3 \Web \intern \E3a \dataprocessingdb \scripts \custom_scripts \Histogram_Correlation.m`

4.6 FIT QUALITY

The codes incorporate a method to calculate the rmse value for every pixel (that is not deleted by the cut mask). These values are averaged over all the pixels of the image to give an estimate of the quality of the fit.

The Root Mean Square Error(RMSE) formula is as follows:

$$RMSE = \sqrt{\frac{\sum_i (y_i - \hat{y}_i)^2}{N}} \quad (4.7)$$

and this fit is calculated for every pixel and averaged over all the pixels to give a quantitative measure of the fit.

R^2 values cannot serve as a measure of the fit as the R^2 is purely a measure of a linear fit and hence cannot be utilised for the inversion recovery fit, which cannot be linearised even using a log plot.

There exists a statistical tool known as the Adjusted R^2 to determine the quality of fit of a polynomial function. This adjusted R^2 incorporates the degree of the polynomial in the formula of the calculated adjusted R^2 . The order of an exponential, being infinite is ill-defined in Adjusted- R^2 .

4.7 SINC PULSE CALIBRATION

In order to apply a perfect $\pi/2$ or π pulse it is important to calibrate the sinc soft pulse so as to apply an accurate RF pulse. This can be done by incorporating Flash imaging and equation [4.1](#)

By incorporating a short TE(echo time) and large TR(repetition time), we can make the signal from a Flash image to be solely dependent on the $\sin(\alpha)$. Thus by varying the aSinc90 amplitude we can vary the flip angle, α and thus generate a Rabi curve. From this, by extracting the asin value of the largest amplitude point, we can calibrate that value to be a flip corresponding to $\pi/2$.

Thus if we wish to implement a flip of a general angle θ , we could use the below formula to calculate the aSinc value of the angle:

$$aSinc(\theta) = \sin(\theta) * aSinc(\pi/2) \quad (4.8)$$

Where $aSinc(\pi/2)$ is chosen to be the value at the highest amplitude [\(4.12\)](#).

The following images give a basic graphical description of the above process.

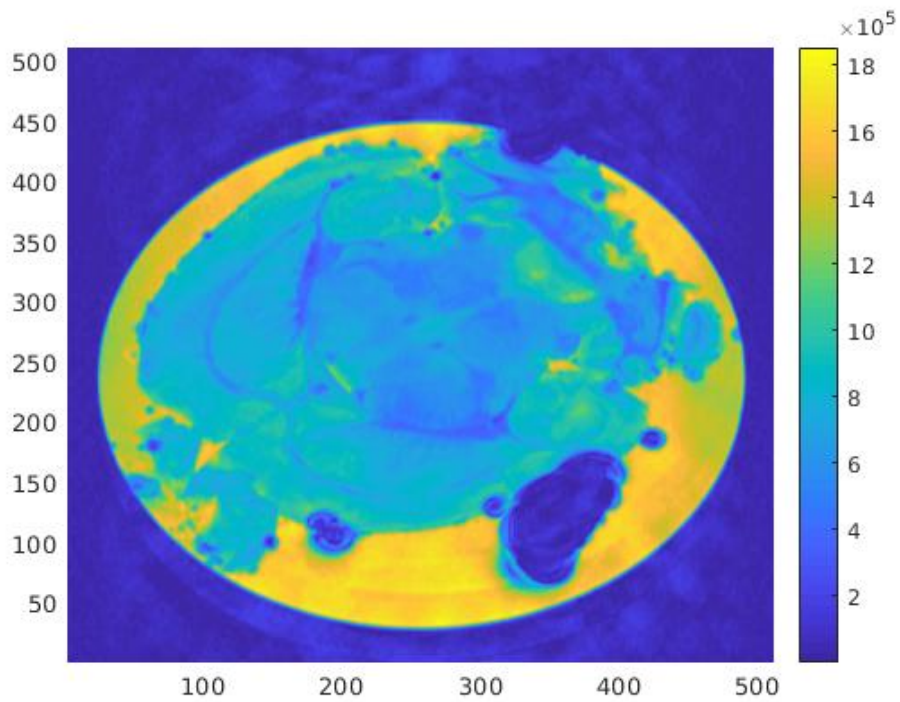


Figure 4.8: High Resolution (512x512) Flash image, TE(echotime)=20ms

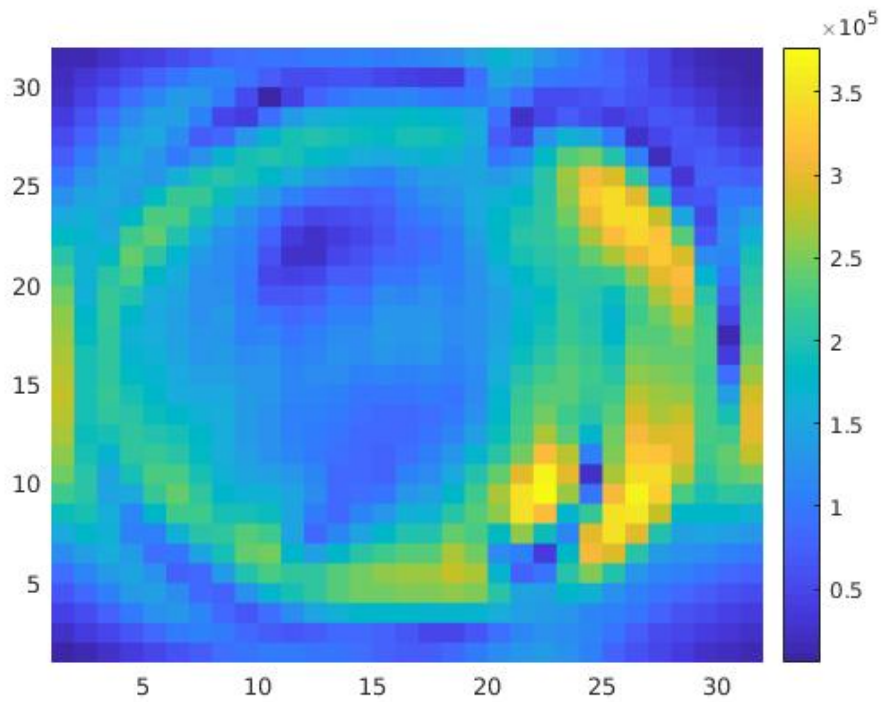


Figure 4.9: Low Resolution (32x32) Flash image, TE(echo time)=20ms. Four points chosen from the blue(Brain) and four from the yellow(formalin).

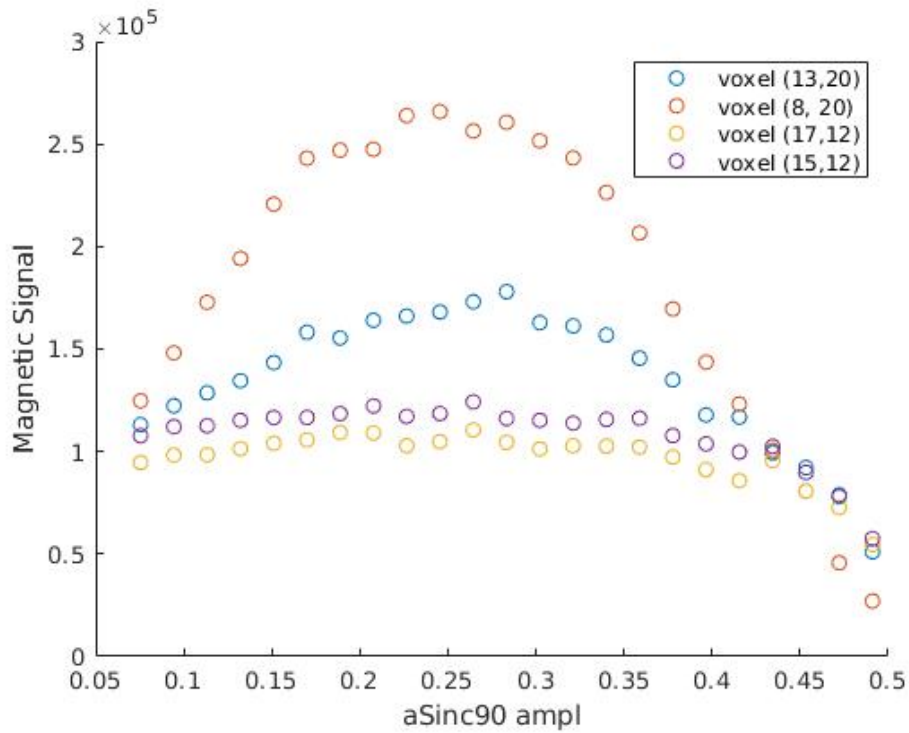


Figure 4.10: four pixels' Rabi Curve from region within the Brain

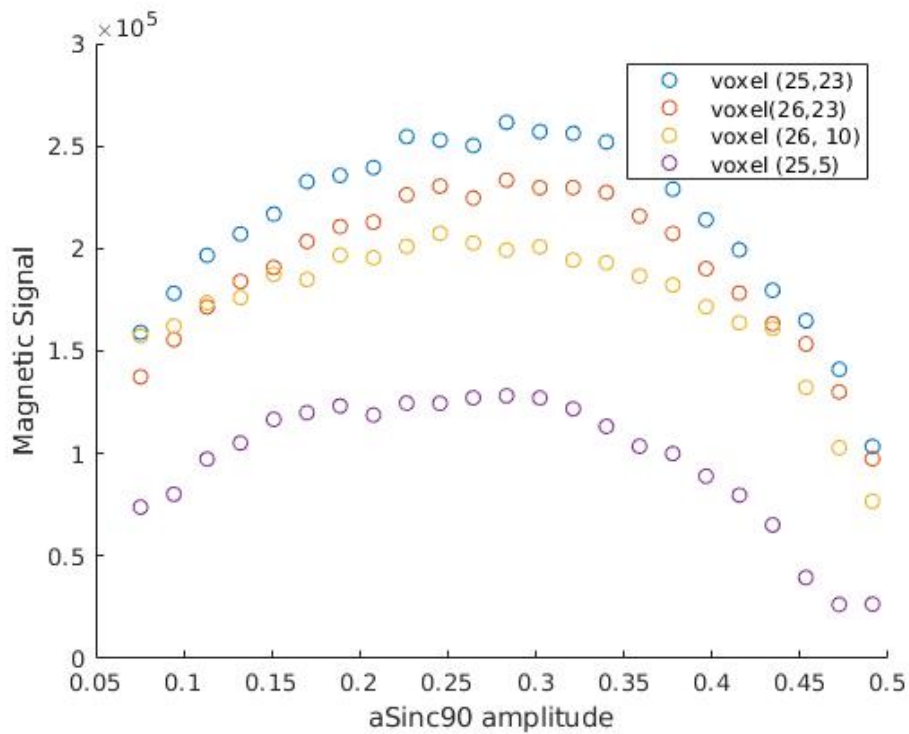


Figure 4.11: four pixels' Rabi Curve from region within the formalin

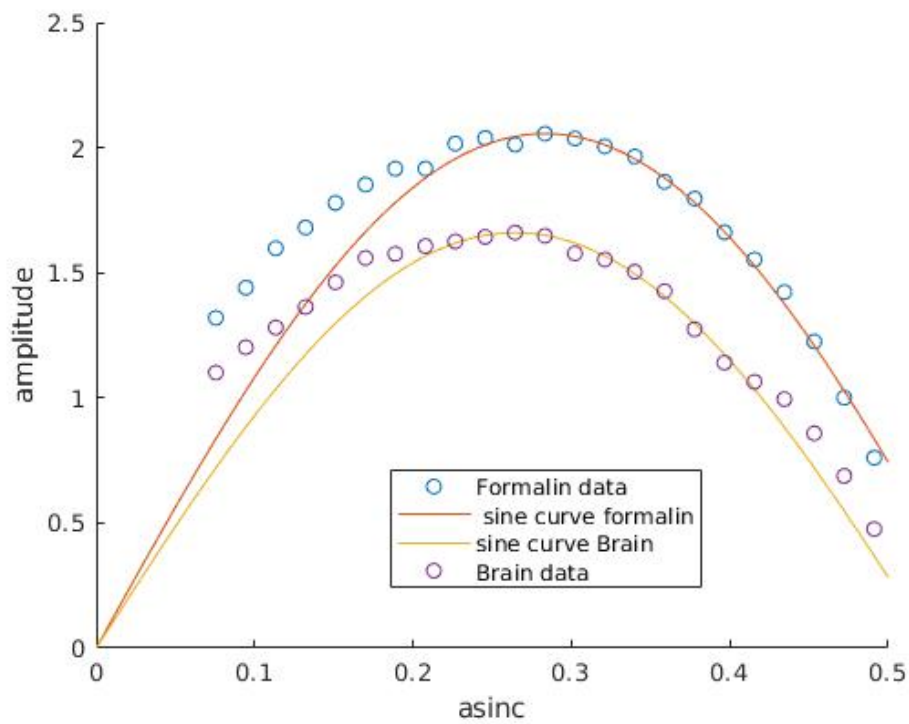


Figure 4.12: Average of the four pixels taken from within the region of the brain and formalin each. The sine Curve corresponding to the maximum value of the Rabi Curve. The more points are averaged, the better the curve fits the data points. One also observes a larger signal from the formalin as compared to the brain[see discussion].

5 RESULTS

5.1 PARAMETER SHORTHAND:

- TR: Repetition Time
- TE: Echo Time
- Twait: Evolution time between the saturation and read pulses in FlashChem imaging.
- SLTk: Slice thickness. (the thickness of slice measured).
- FrSl: Frequency slice. (The slice selected was at that particular frequency (due to the z gradient) along the z direction.
- BW=Bandwidth. Always 5KHz (which implies the Z gradient strength is $5\text{KHz}/\text{SLTk}$).

5.2 IMAGE DETAILS:

- **Specimen:** mouse brain.
- **Solution:** 10 percent Formalin solution, which corresponds to 4 percent Formaldehyde in distilled water. We would for convenience refer to it as simply formalin, henceforth.
- **Field of view:** 16mm. This corresponds to the width and length of the region portrayed. In a 256x256 pixel image, this implies that the size of a single pixel was $16/256=0.0625\text{mm}$ in dimension (length and width).
- The brain sample was placed in a 15mm test tube, with the brain on the transverse plane and all cross sections accordingly are in the transverse direction.

5.3 T1 MAPS

Location of Flashchem pulse sequence for 600MHz: https://qnap.e3.physik.tu-dortmund.de/intern/E3a/pulseprogrammdb/NMR_600_FlashChem/pulse_data_base.php This webpage contains the Pcode which when compiled on the 600MHz system, can be used to run FlashChem from within Spinsight.

5.3.1 T1 MAP AT 400MHZ SPECTROMETER

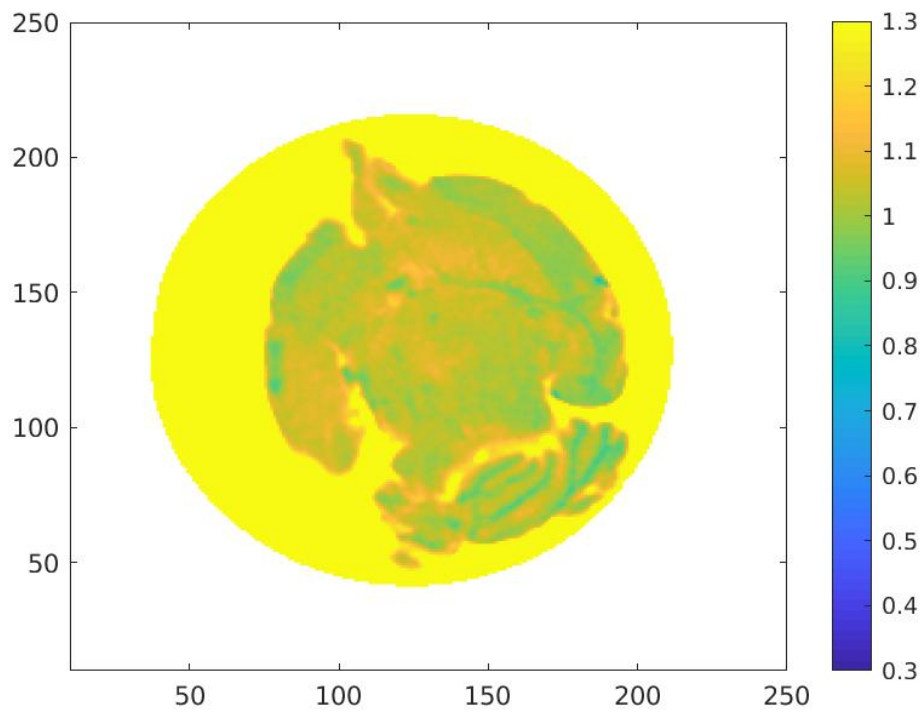


Figure 5.1: T1 map (in seconds) using Flash at 400MHz, with detailed contrast

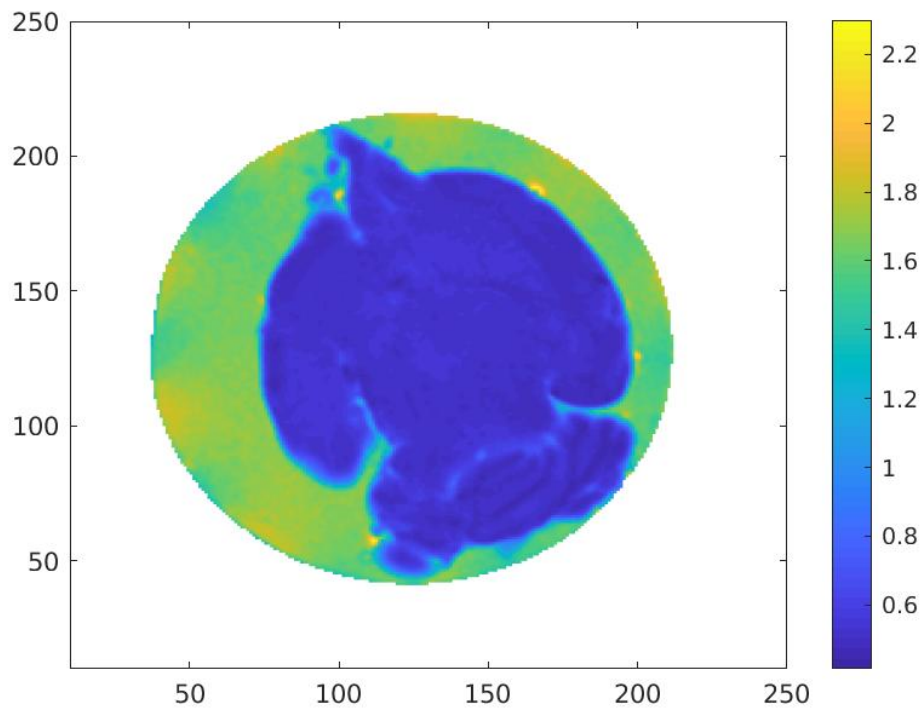


Figure 5.2: T1 map(in seconds) using Flash at 400MHz, with lower contrast. SITk=0.4mm

It is noticed from the images [5.2](#) that there is visible T1 contrast between the liquid solution in which the brain sample is placed as well as within regions of the brain. This is in line with what we would expect in the brain, consisting primarily of two tissues, Grey and White matter. White matter having generally lower T1 values [\[11\]](#) can be noticed in the darker bands in the brain and are located in deeper subcortical channels.

In the forthcoming images, I utilise more statistical and visualisation tools to both better interpret data as well as to test the validity of such maps. These tools include:

- Use of histogram plots to better differentiate between different T values. This involves tallying up the number of pixels that exhibits a particular range of T_1 , T_2 or T_2^* values.
- Use of root mean square value of a fit. This helps us judge the quality of a fit and thus compare results from two or more experiments.
- Plot of the fitted function with data points for a few pixels in the image.

5.3.2 T1 MAP AT 600MHZ SPECTROMETER

Image-1

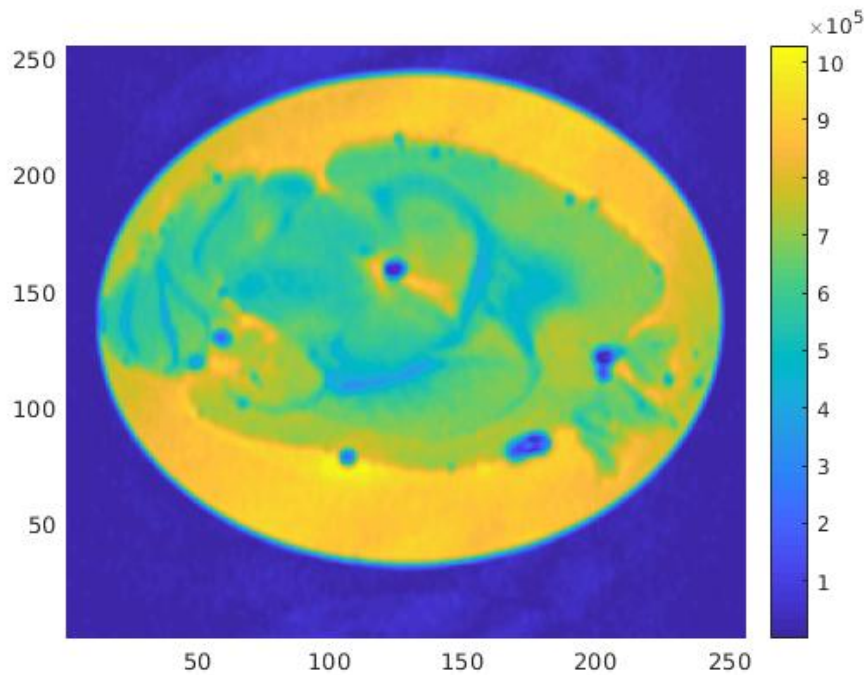


Figure 5.3: Signal Image for Twait of 20ms ,(Flashchem) at 600MHz. SITk=0.5mm, FrSl=0.0Hz

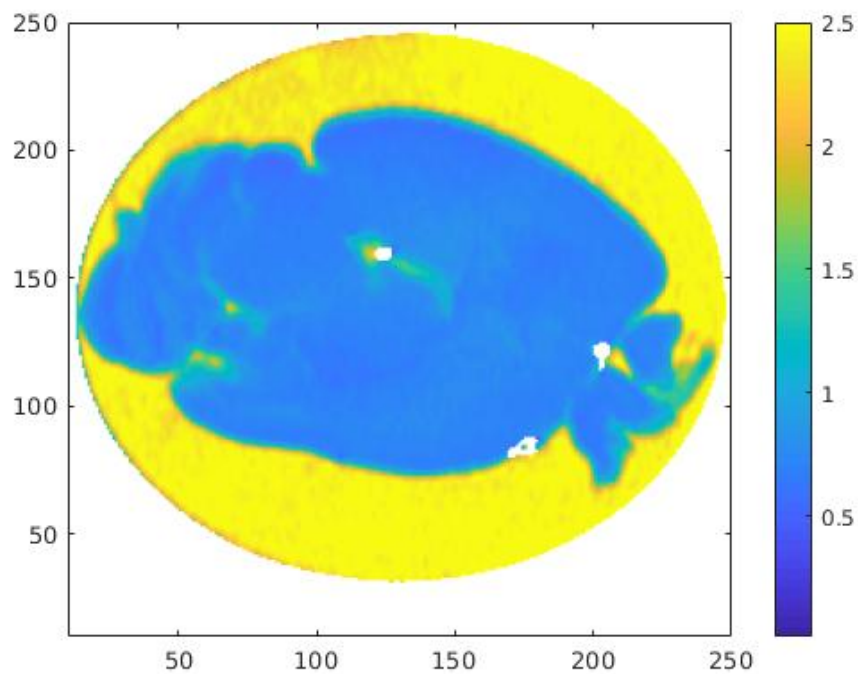


Figure 5.4: T1 map(in seconds) of the above slice using Inversion Recovery (Flashchem) at 600MHz

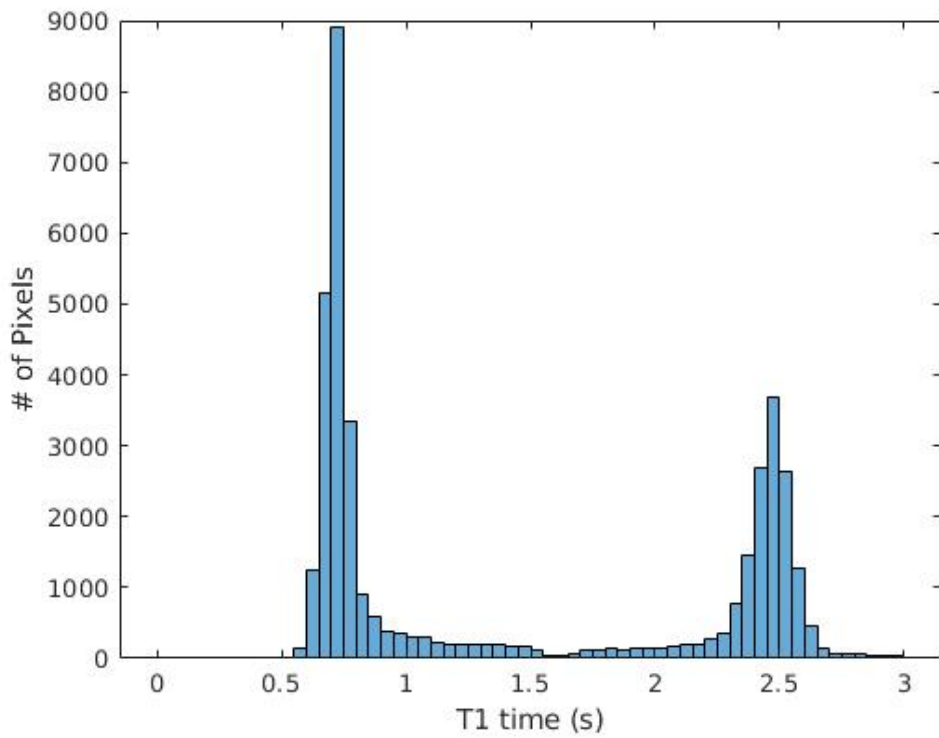


Figure 5.5: Histogram of the above T1 map. We notice two large bins:0.70-0.75s and 2.45-2.5s

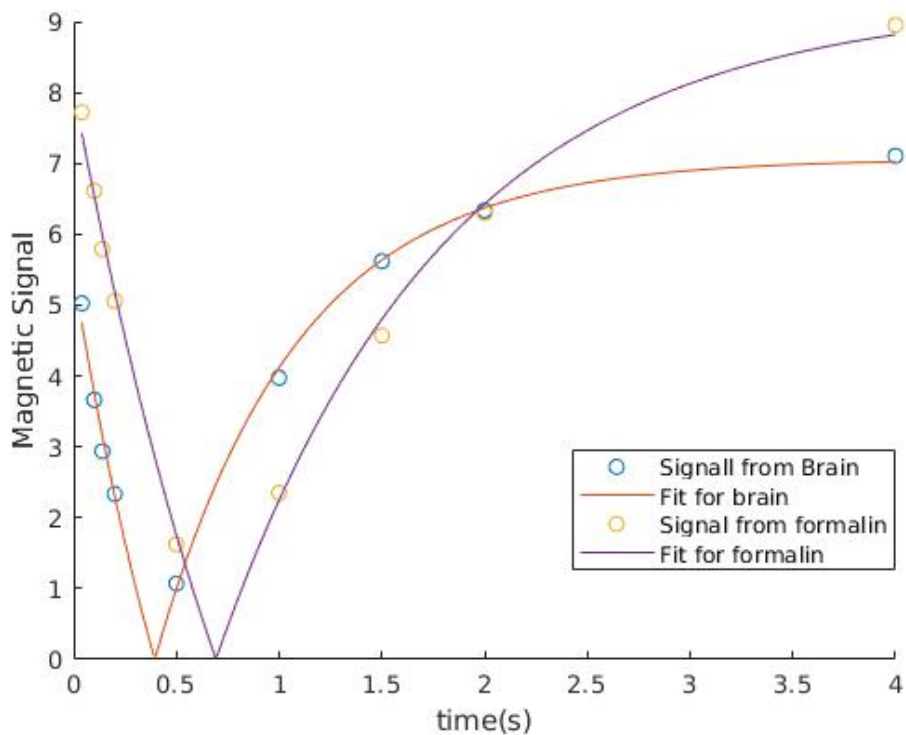


Figure 5.6: T1 Fit of the two primary regions(Brain and Formalin) that we observe. Average RMSE=0.11

Now we focus on a different slice of the brain sample:

Image-2

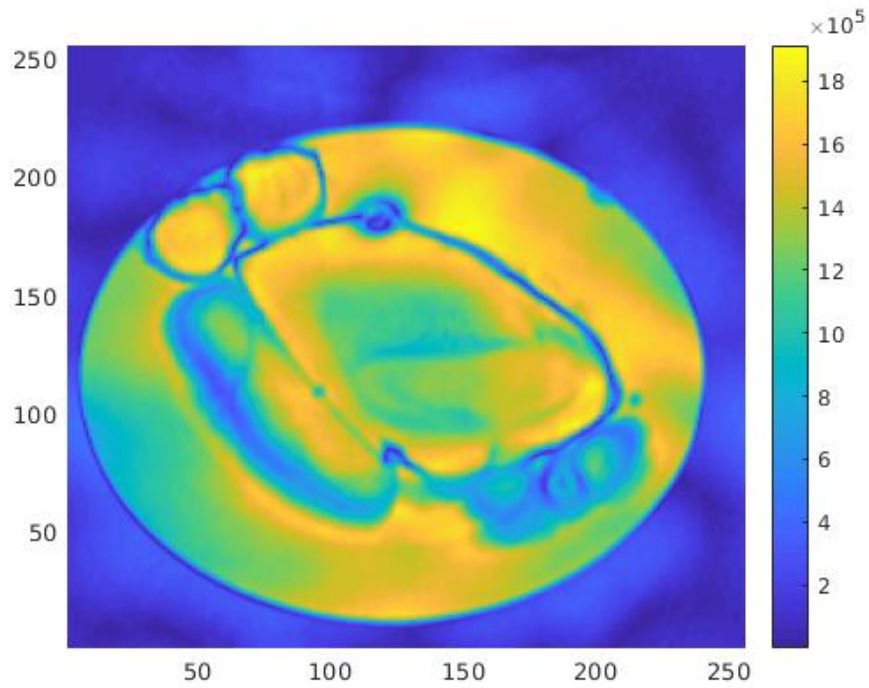


Figure 5.7: Signal Image for Twait of 400ms ,(Flashchem) at 600MHz. SItk=1.0mm, FrSl=-4000.0Hz

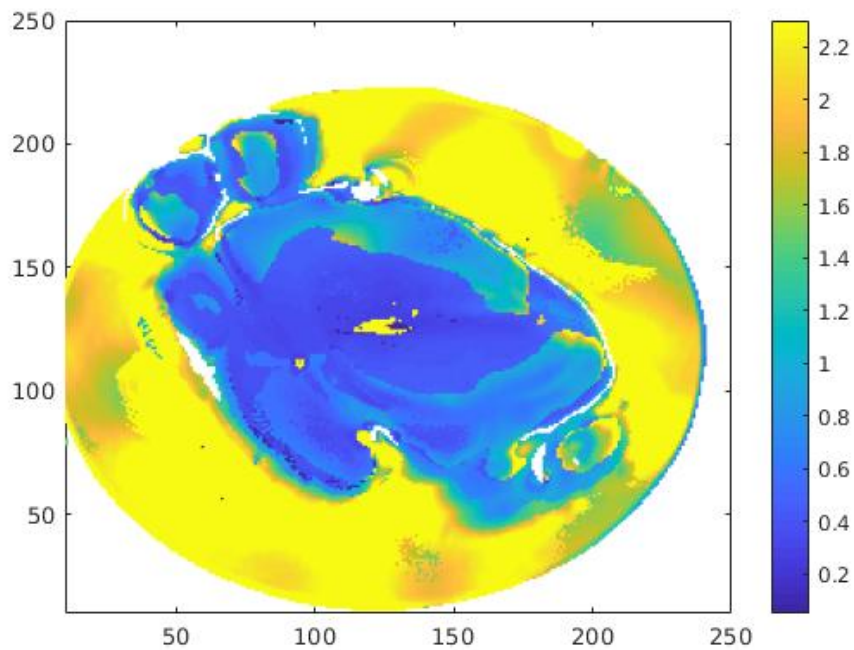


Figure 5.8: T1 map(in seconds) using Inversion Recovery (Flashchem) at 600MHz

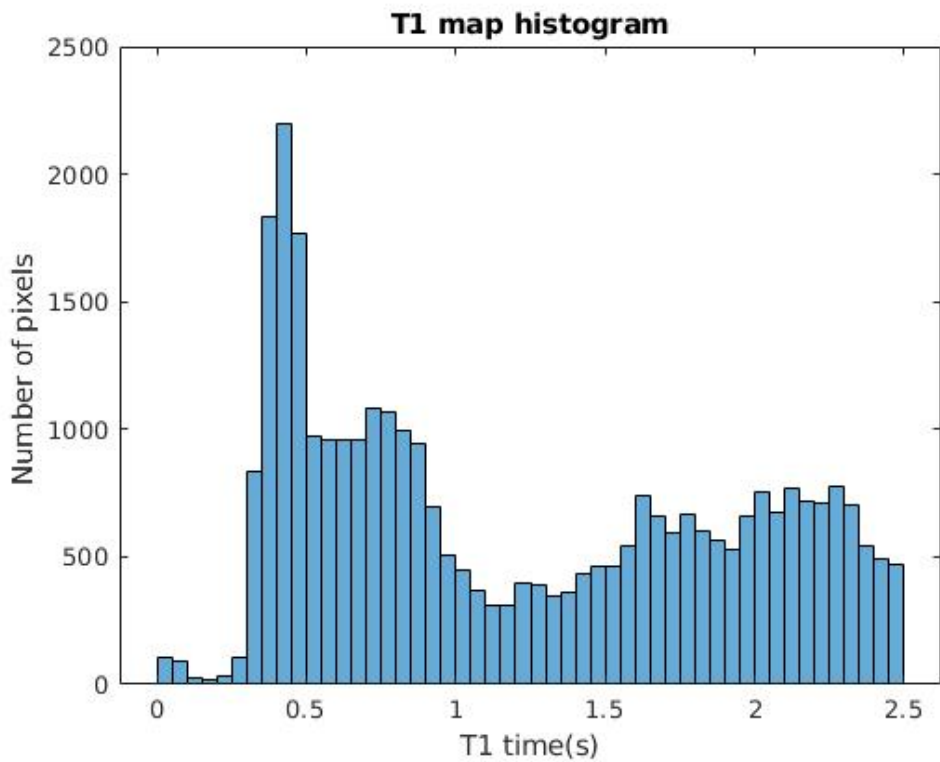


Figure 5.9: Histogram of the above T1 map. We notice roughly four large bins: 0.45-0.5s (white matter) and 0.7-0.8s (grey matter), 1.6s and a peak beyond 2s (formalin).

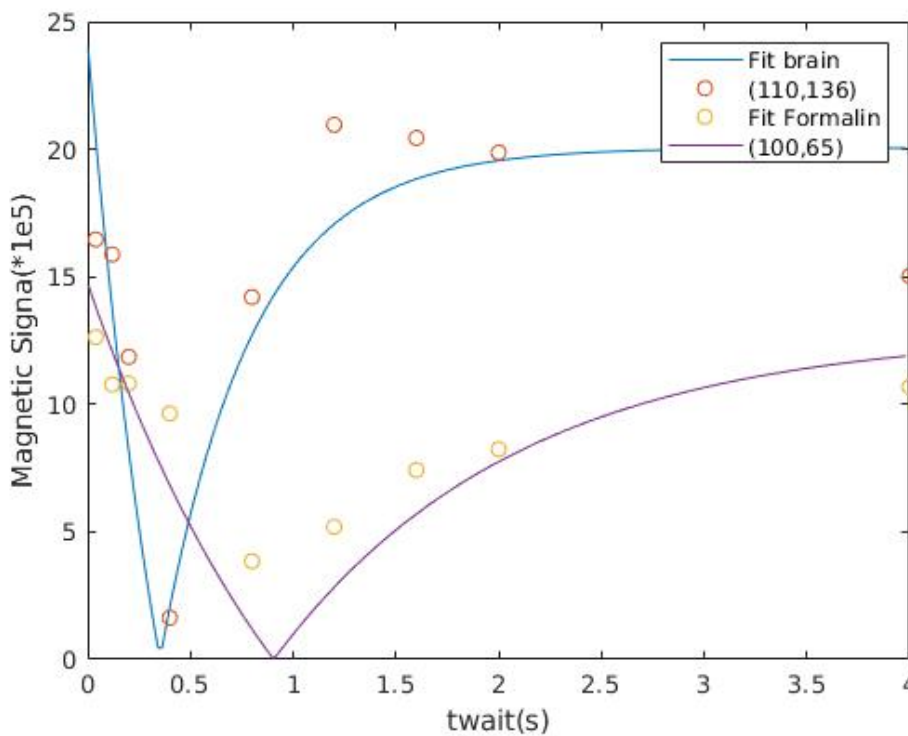


Figure 5.10: T1 Fit of the two primary regions that we observe. Average RMSE=2.83 (error in this experiment discussed in chapter 6).

Image-3

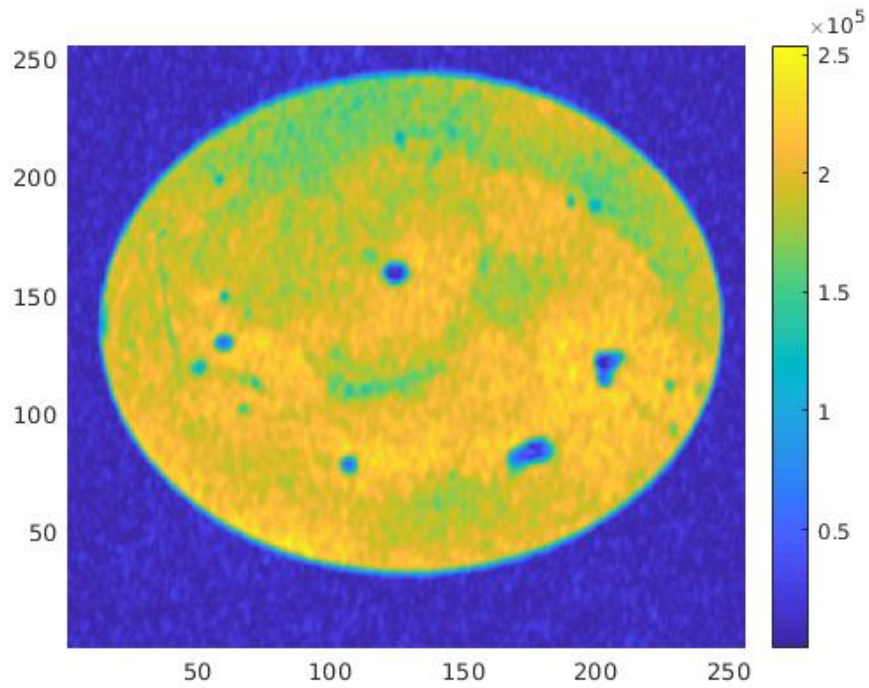


Figure 5.11: Signal Image for Twait of 20ms ,(Flashchem) at 600MHz. SlTk=0.5mm, FrSl=0.0Hz

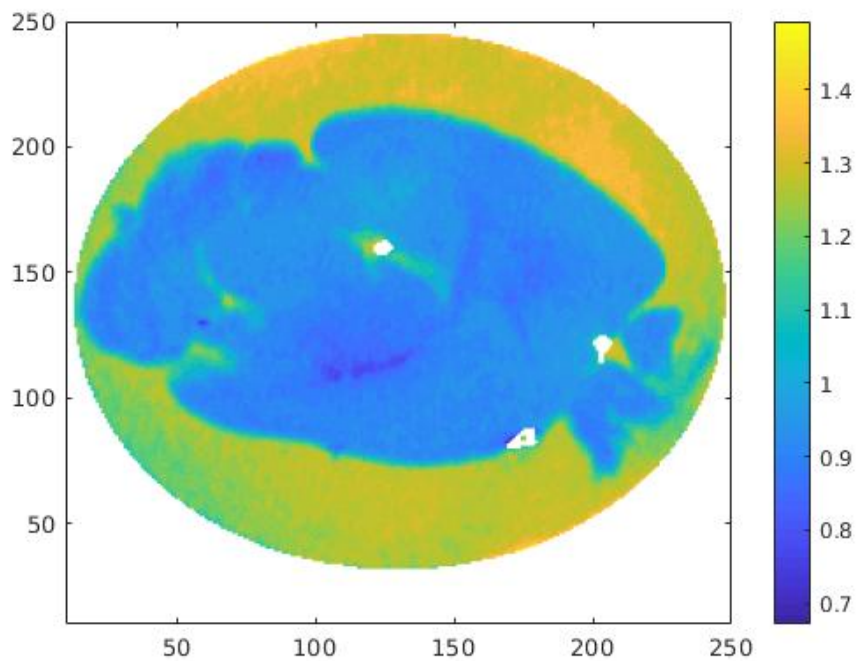


Figure 5.12: T1 map(in seconds) using Saturation Recovery (Flashchem) at 600MHz

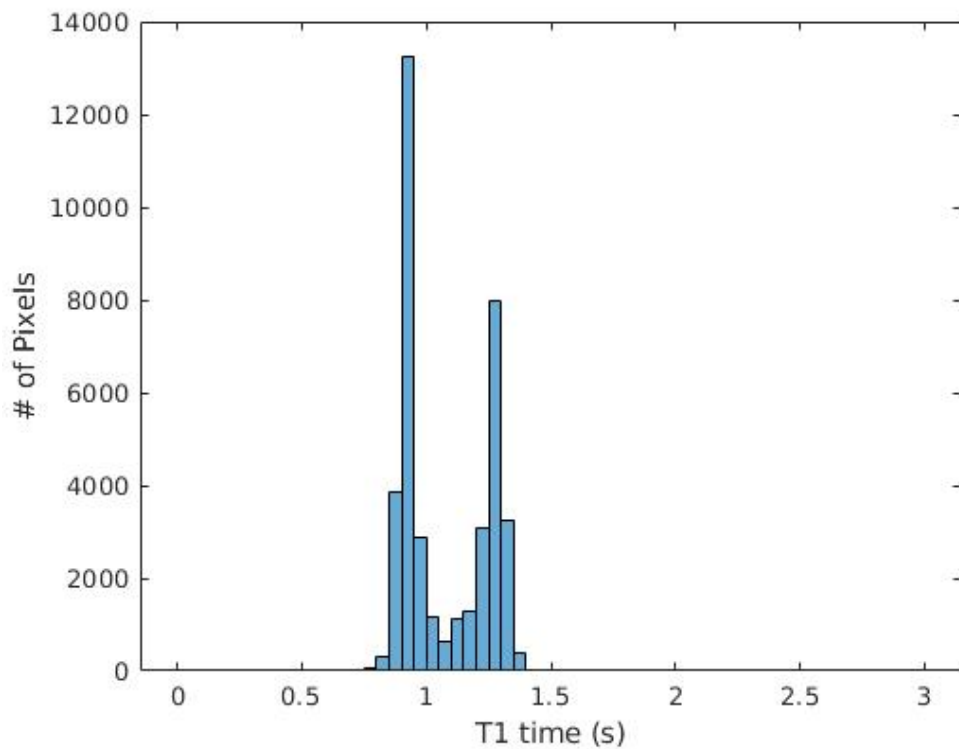


Figure 5.13: Histogram of the above T1 map. We notice roughly two large bins:0.9-0.95s (Brain) and 1.3-1.35s. This could possibly correspond to the two middle peaks in figure 5.9. Since saturation recovery as previously mentioned, performs poorly in characterising different T1 values as compared to inversion recovery, we could expect this behavior(where certain peaks remain unresolved).

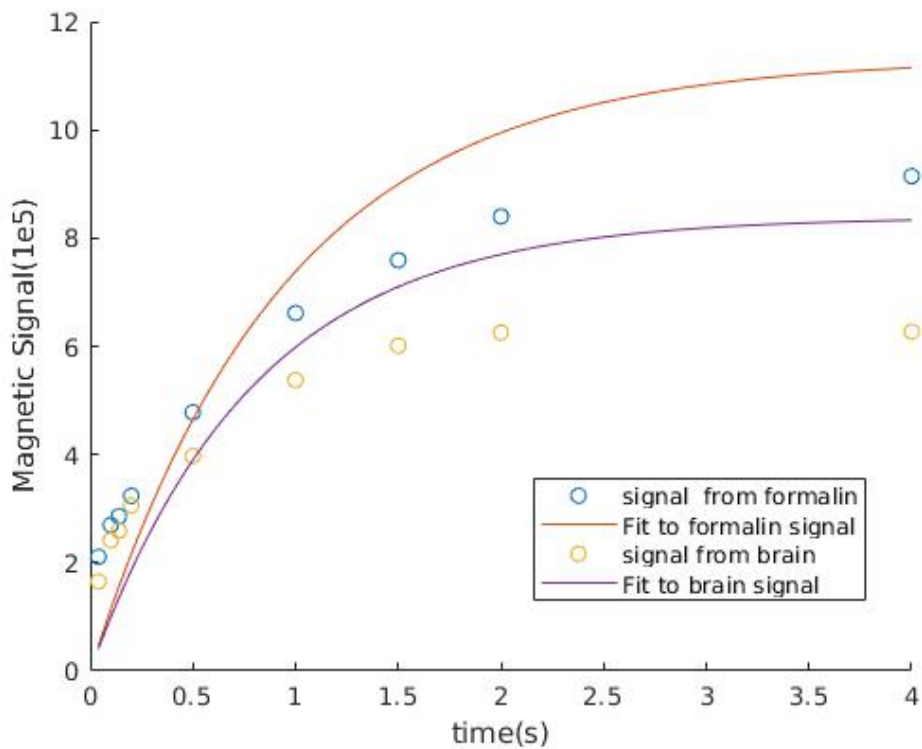


Figure 5.14: T1 Fit of the two primary regions that we observe. Average RMSE=1.27

5.4 T2 MAPS

Image-4

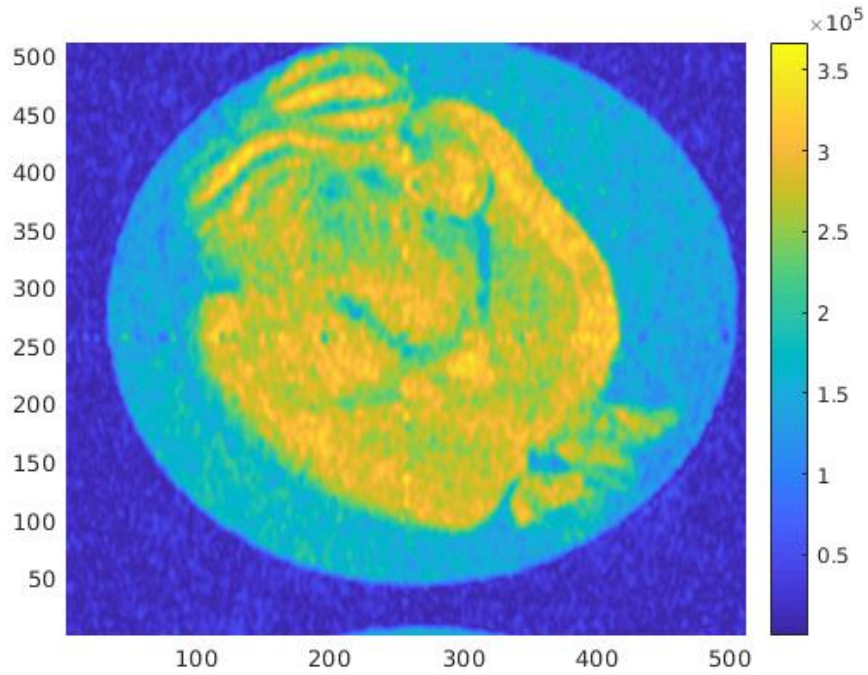


Figure 5.15: Signal Image for TE of 12ms, (Spinwarp) at 600MHz. SItk=3.0mm, FrSl=-1500.0Hz

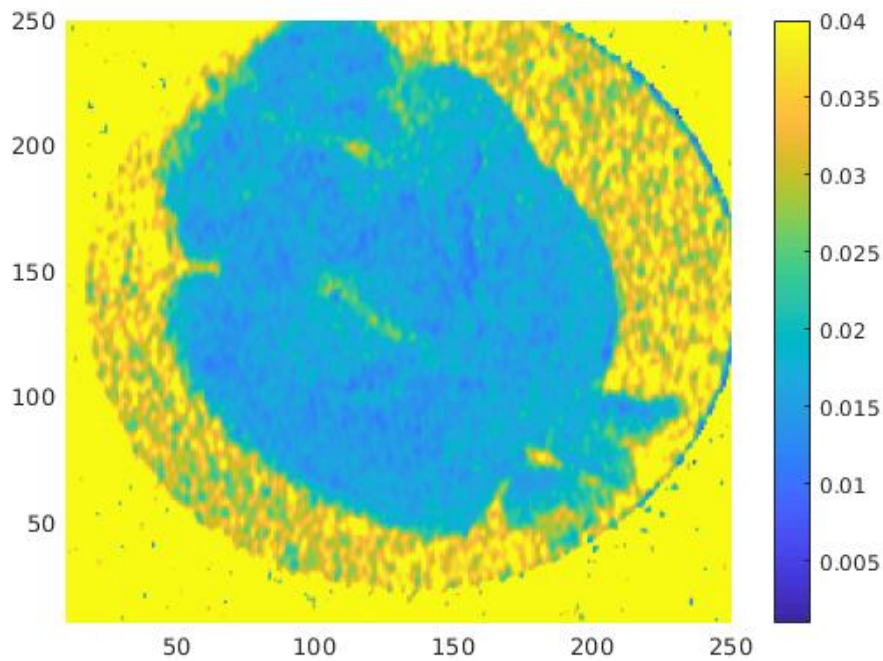


Figure 5.16: T2 map(in seconds) using Spinwarp at 600MHz

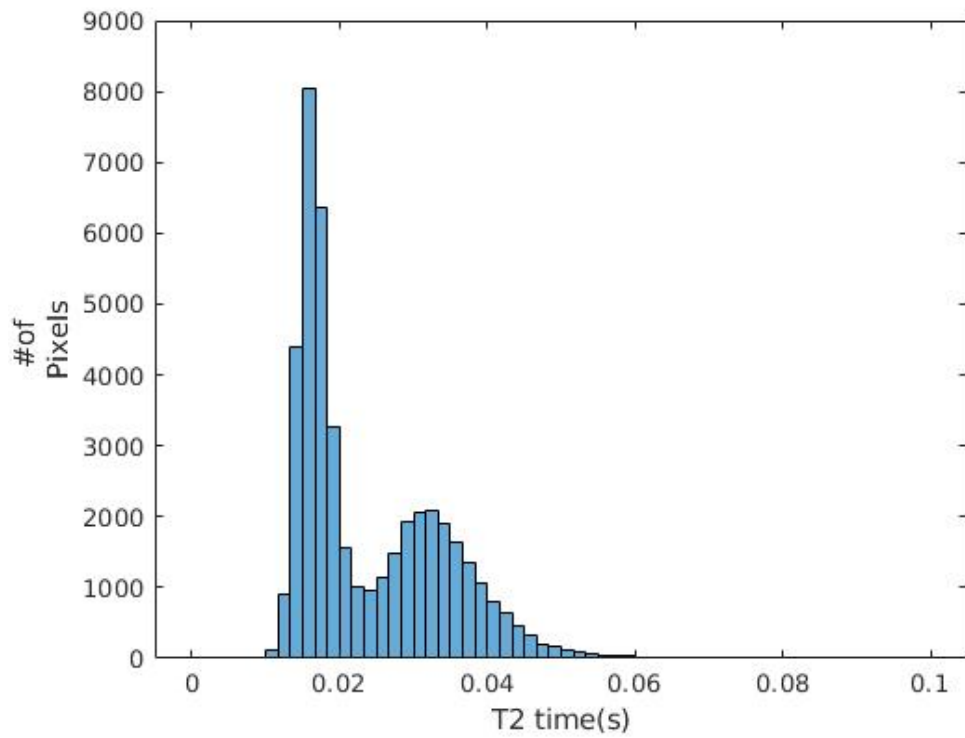


Figure 5.17: Histogram of the above T2 map. We notice two prominent bins: one at 15-17ms from the region in the Brain and another 30-35ms from the region of the formalin.

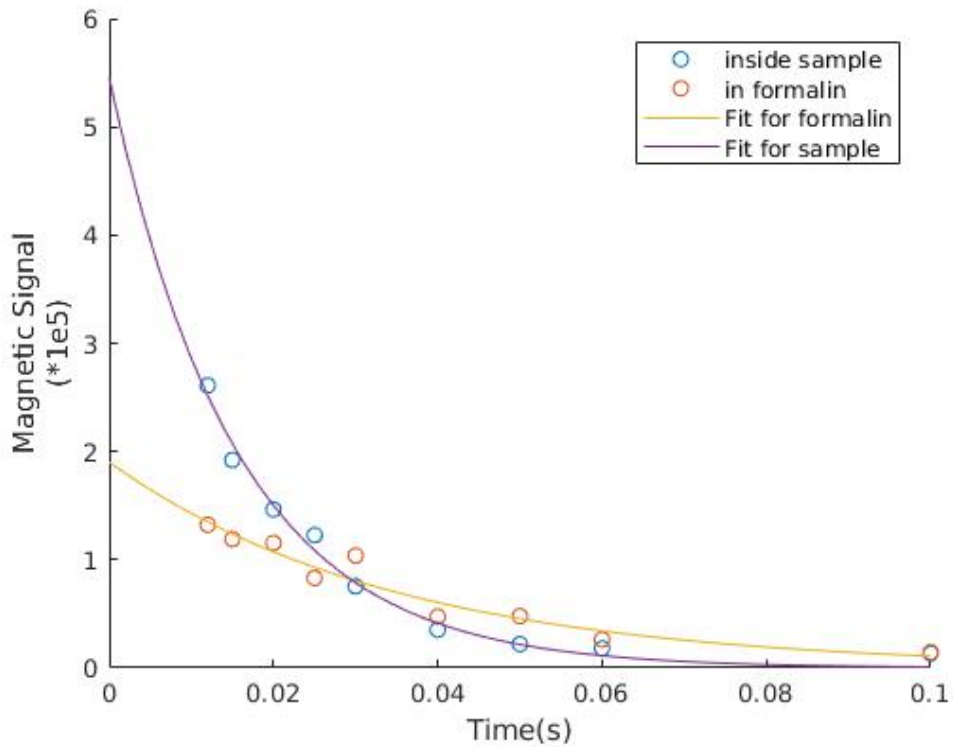


Figure 5.18: T2 Fit of the two primary regions that we observe. RMSE=0.12

5.5 T_2^* MAP

Image-5

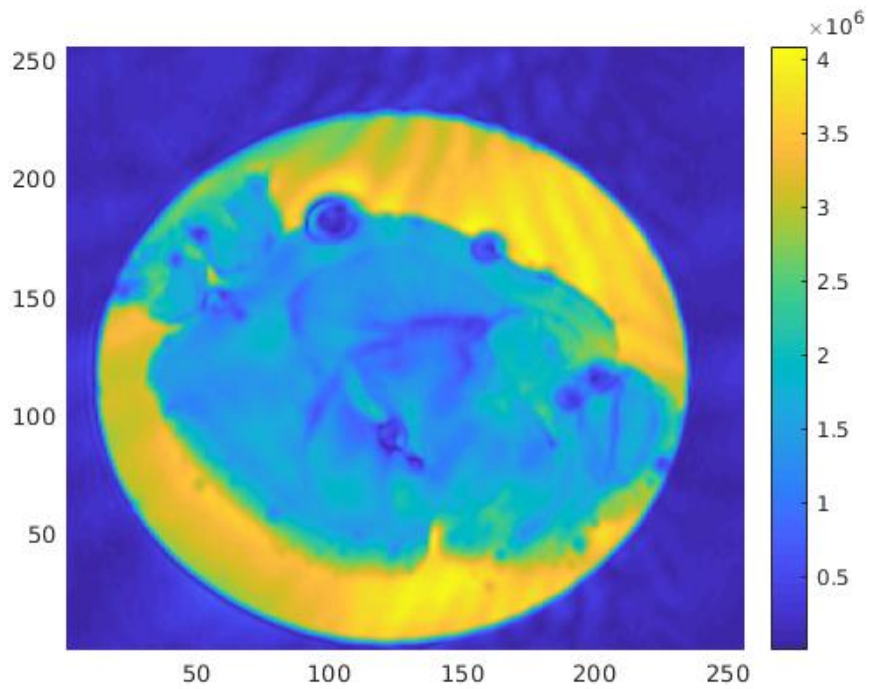


Figure 5.19: Signal Image for TE=20ms , Flash at 600MHz. Sltk=1.0mm, FrSl=-4000.0Hz

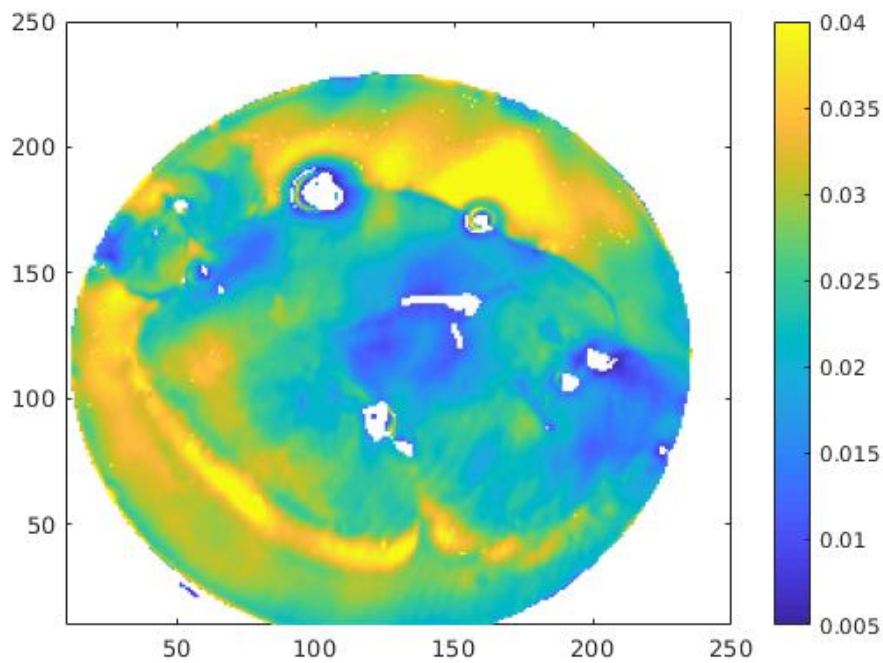


Figure 5.20: T_2^* map (in seconds) using Flash at 600MHz

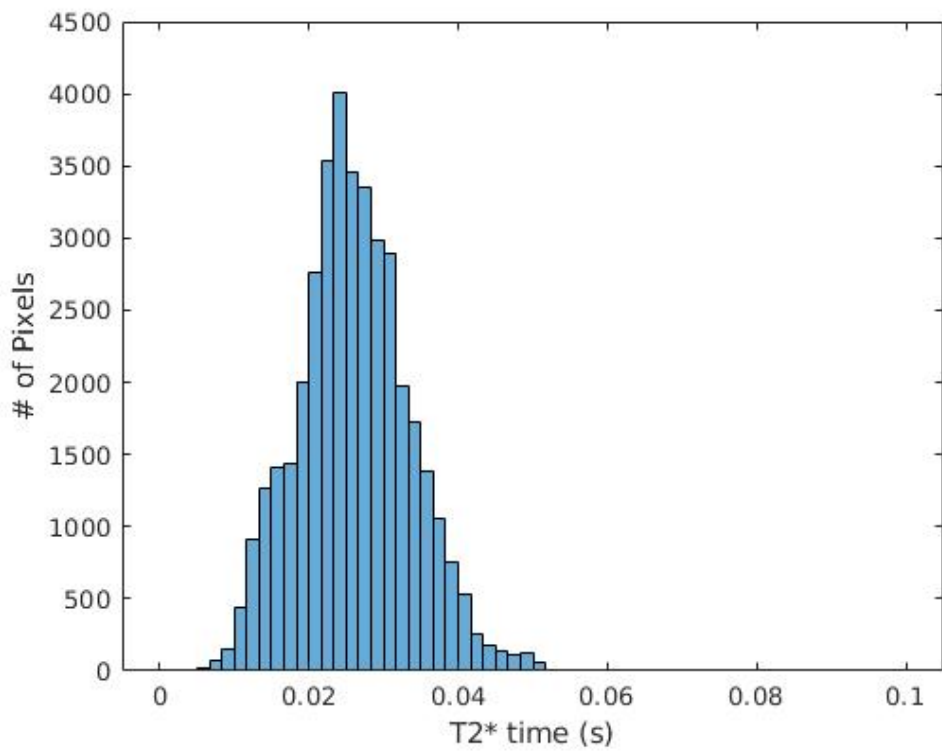


Figure 5.21: Histogram of the above $T2^*$ map. We notice just a single peak at 20-25ms.

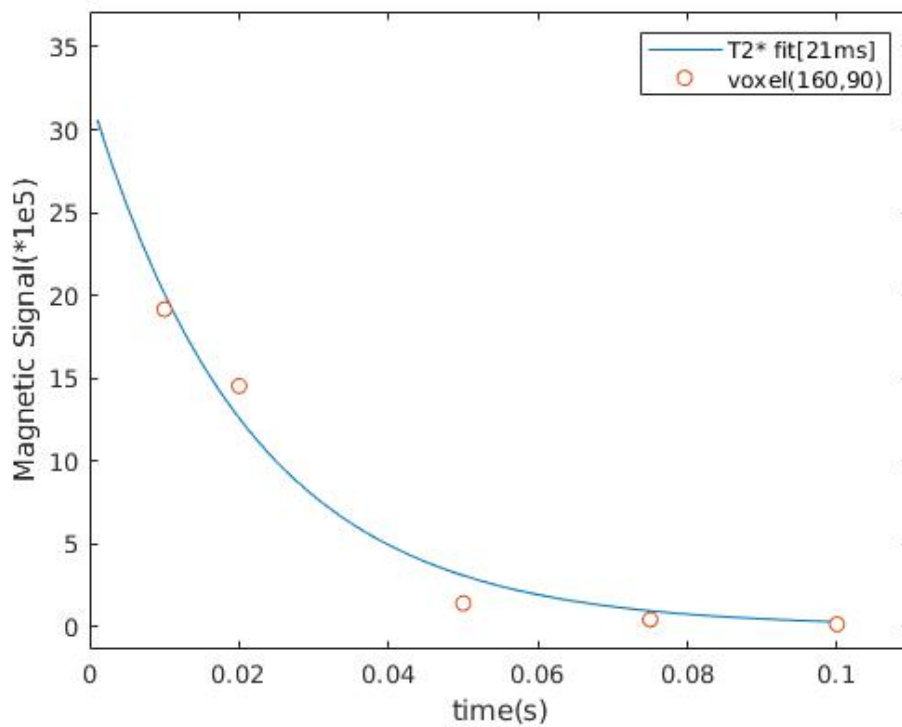


Figure 5.22: $T2^*$ Fit of the central region that we observe. RMSE=1.19

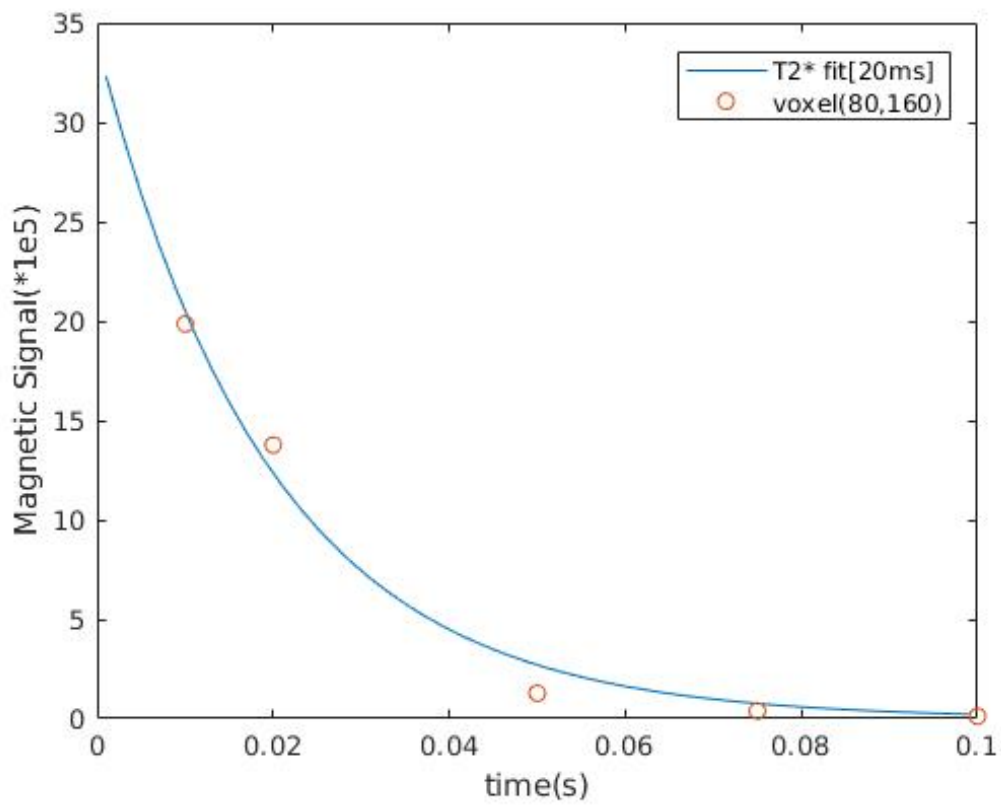


Figure 5.23: Plot fit 2

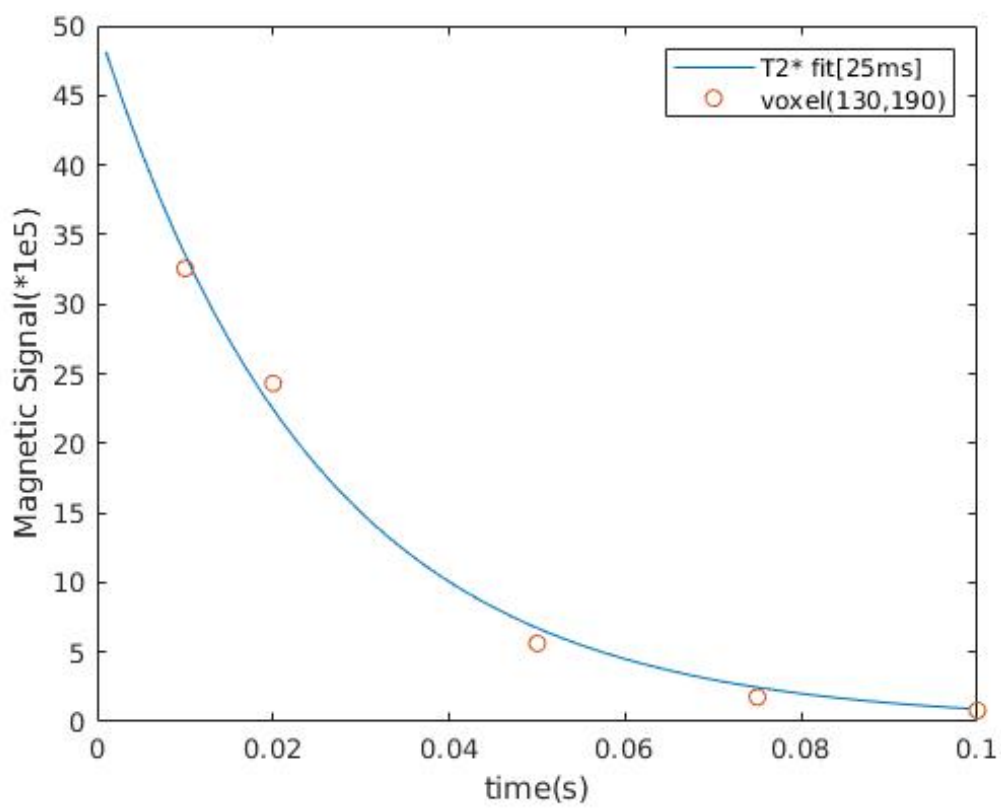


Figure 5.24: Plot fit 3

6 DISCUSSION

6.1 TRENDS

From the results across all the three types of maps and its various experiments, we can infer the following:

- There is an obvious contrast between the tissue and the formalin solution (in which the sample is prepared), with the formalin solution having higher T1. This is to do with the fact that water molecules in formalin are less bound to molecular structures and thus have a higher tumbling rate. This in turn leads to a higher T1 value.
- A similar pattern is noticed in T2 maps, although the reason for a similar observation differs. Water (hence free hydrogen protons), bound to larger molecular structures, in the brain tend to realign slowly due to larger intrinsic field. Thus T2 values seem to be higher in the formalin as opposed to tissues within the brain.
- Not all slices considered had a similar proportion of grey and white matter. This was evident by the lack of double peaks (within the expected time values) in the histogram plots for many slices.
- T1 maps seem to provide a better method to distinguish different tissues as seen in **Image-2** (5.8) and from the image obtained from the 400MHz (5.2). This could be in part due to the larger range of values of T1 as opposed to T2 values.
- We also notice in most Magnetic Signal images, that the signal from the formalin (due to a higher Hydrogen proton concentration) is higher than that from the brain. Exception: **Image-4**. This is due to a higher concentration of Hydrogen atom concentration in the formalin than in the brain and hence a higher magnetic signal.
- An increase in accuracy of the fit (lower root mean square error) corresponds to better defined T1 and T2 separation by means of defined peaks in the histogram plot.

6.2 SOURCES OF ERROR

- A smaller slice thickness results in a more precise map as the thicker the slice, the more the signal is averaged out over the slice, losing the detailed structure within each pixel.
- In inversion recovery, it is important to have at least five points between $0.25T_1 - 3T_1$. This is to account for at least two points before and after the 'kink' (non-differentiable minima of the curve) and at least one point in the vicinity of the minima.
- In [5.8](#), subtle rotations between the different acquisitions were noticed. This could be the reason for a 'smeared' effect in the T_1 map. It could also have lead to gradual spread of the peaks in the histogram plot and the incorrect signal magnitude of the formalin solution with respect to that from the tissue. Below, I have analysed effects of the same. The problem was later resolved by tightening the screw cap on the probe head that was loose and which thus failed to hold the sample tube in position.
- Another possible cause of error in fig 5.10, could be the choice of the pixel. Pixel (100, 65) could be on the border region between the brain and formalin (as observed from fig 5.8) and thus could be the relaxation curve of brain tissue as opposed to that of formalin as claimed.

6.2.1 ROTATION ERROR

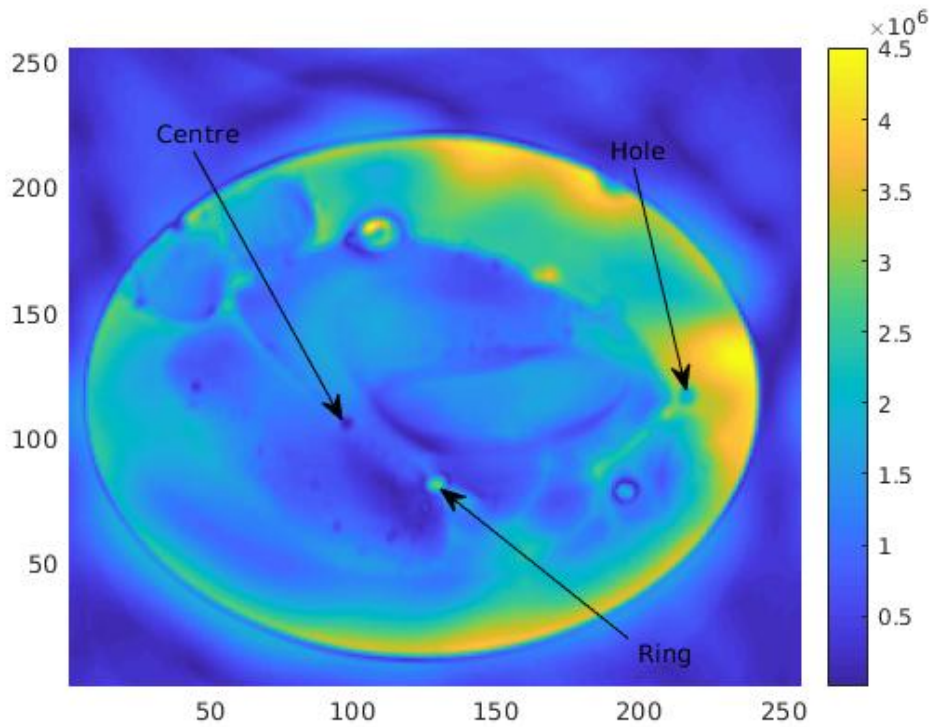


Figure 6.1: Markers used to track rotations

The position of the various markers were tracked (through their pixel locations). These were plotted for the changes in both the X and Y directions.

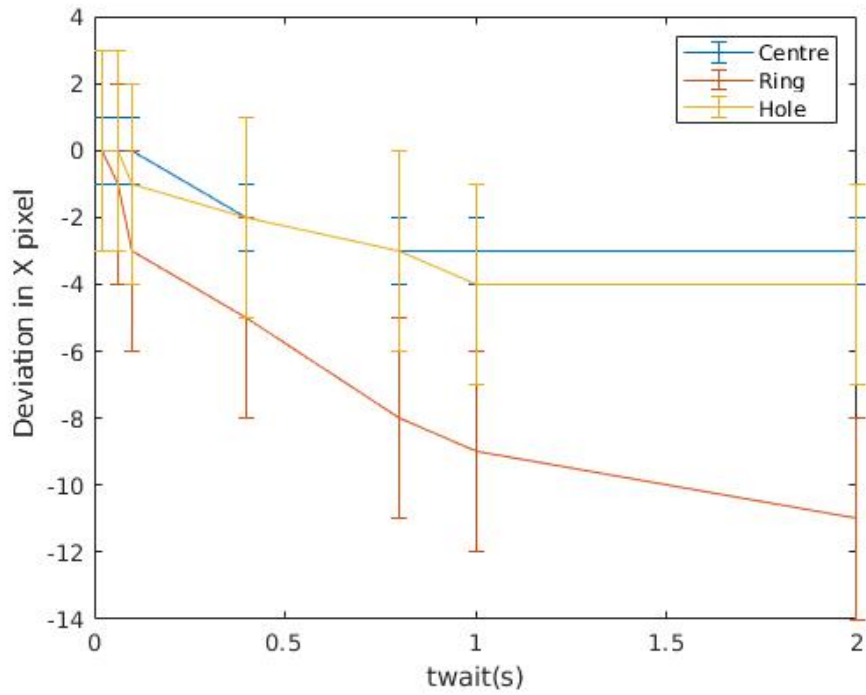


Figure 6.2: X pixel changes over different acquisitions (twait values).

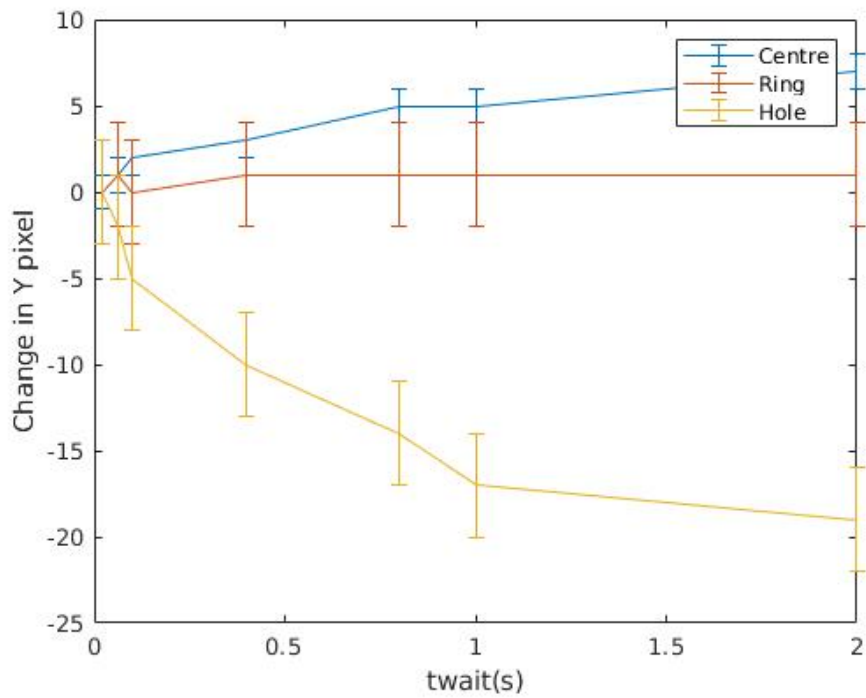


Figure 6.3: Y pixel changes over different acquisitions (twait values). At larger twait times, the pixel moves almost a millimeter in distance (sixteen pixels). This problem was eventually resolved by securing the tube in place within the probe head.

7 CONCLUSION

Thus from this thesis, the use of T maps was used to bring about contrast between specific tissues, namely grey and white matter. Every aspect of the measurement process was explored and noted in this thesis, right from the theory, the imaging pulse sequence used, processing scripts and the underlying algorithms, eventually culminating in the observation made.

Based on the known locations of Grey and White matter in the brain as well as their relative T values, we were able to identify regions in the brain that show a difference in T values and correlate them to the location within the slice, through the relaxation colourmaps.

This research can be extended to have more powerful diagnostic relevance. This can be done by harnessing the combined power of T1 and T2 maps. This could be implemented by means of a correlation map, where we can extract the T1 value on one axis and the T2 on the other. This will help us differentiate between Grey and White matter on two dimensions (T1 and T2) as opposed to just one (T1 or T2). Such contrasts and visualisation techniques could be particularly useful in studying tumours and identifying highly metastasizing cells, which tend to possess a different T1/T2 value from the surrounding cells [12].

Another useful method, which I had begun but was unable to complete would be CPMG imaging. CPMG, being a useful tool in dynamical decoupling would help improve the signal to noise ratio, which would then help develop better contrasts as well between tissue structures.

Further these CPMG images could be used in conjunction with T1 and T2 maps so as to develop a correlation map, which as explained above, would enhance our ability to develop accurate contrast mechanisms to differentiate between tissues.

All these developed imaging techniques cannot be directly applied in a clinical setup, due to the extremely long run times and unregulated SAR values. However the experiments run serve as a basic Proof of Principle, which could be optimised for a more advanced clinical setup.

REFERENCES

- [1] Basser P J, Mattiello J, LeBihan D; *MR Diffusion Tensor Spectroscopy and Imaging* **66** 259-267 (1994).
- [2] Taylor D G, Bushell M C *Phys. Med. Biol.* **30** 345.
- [3] F. Bloch, *Nuclear Induction*, *Phys. Rev.* **70**, 460-474 (1946).
- [4] D.D. Traficante, *Can T2 be longer than T1?*, *Concepts in Magnetic Resonance* **3**, 171-177 (1991).
- [5] R.K. Wangsness, and F. Bloch, *The Dynamical Theory of Nuclear Induction*, *Phys. Rev.* **89**, 728-739 (1953).
- [6] A.G. Redfield, *On the Theory of Relaxation Processes*, , *IBM Journal of Research and Development* **1** 19-31 (1957).
- [7] A.G. Redfield, *Intramolecular Dipolar Relaxation in Multi-spin systems*, , *Adv. Magn. Reson.* **1** 1-32 (1966).
- [8] M. Goldman, *Formal Theory of Spin-Lattice Relaxation*, *Journal of Magnetic Resonance* **149** 160-187 (2001).
- [9] M.H. Levitt, L. Di Bari, *Bull. Magnetic Resonance* **16** 94-114 (1994).
- [10] T.O. Levante, R.R. Ernst, *Chem. Phys. Letters* **241** 73-78 (1995).
- [11] M.A Dieringer, M.Deimling¹, D.Santoro, J.Wuerfel, V.I.Madai, J.Sobesky , F.V.Knobelsdorff-Brenkenhoff, J.Schulz-Menger^{1,2}, T. Niendorf *Rapid Parametric Mapping of the Longitudinal Relaxation Time T1 Using Two-Dimensional Variable Flip Angle Magnetic Resonance Imaging at 1.5 Tesla, 3 Tesla, and 7 Tesla* **PLoS One** (2014).
- [12] C.Weidensteiner, P.R.Allegrini, M.Sticker-Jantscheff, V.Romanet S.Ferretti¹ and P.M.J.McSheehy *Tumour T1 changes in vivo are highly predictive of response to chemotherapy and reflect the number of viable tumour cells-a preclinical MR study in mice* **BMC Cancer** **14:88** (2014).
- [13] www.mriquestions.com
- [14] http://www.tifrh.res.in/~NMRTIFRH/presentations/Matthias_Ernst-Relaxation-Redfield.pdf
- [15] Library of Pulse Sequences used: <https://qnap.e3.physik.tu-dortmund.de/intern/E3a/pulseprogrammdb>